Master's thesis

NTNU
Norwegian University of Science and Technology
Faculty of Natural Sciences
Department of Physics

Gert Kluge

Simulating Particle Cascades in the Search for Dark Matter using Cosmic Neutrino Observations

Master's thesis in MSPHYS
Supervisor: Michael Kachelriess
June 2019

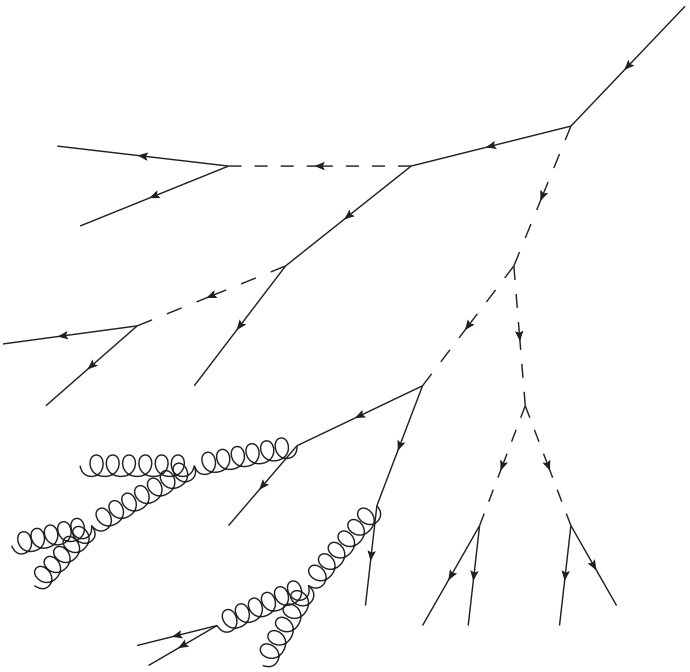

NTNU
Norwegian University of
Science and Technology

Gert Kluge

Simulating Particle Cascades in the Search for Dark Matter using Cosmic Neutrino Observations

Master's thesis in MSPHYS
Supervisor: Michael Kachelriess
June 2019

Norwegian University of Science and Technology
Faculty of Natural Sciences
Department of Physics

Abstract

We present a procedure for simulating particle cascades with applications to dark matter searches and neutrino astronomy. We are motivated by the steady developments at the IceCube neutrino observatory, which have made available unprecedented data on the diffuse cosmic neutrino flux. The case is made for using neutrino data to look for signals of superheavy dark matter decays. We emphasize that superheavy dark matter decays can generally be expected to cause cascading of high-energy particles, involving both strong and electroweak interactions. We build on a cascading formalism from quantum chromodynamics to model the cascading of almost all standard model particles, distinguishing also between left- and right-handed fermions. Monte Carlo algorithms are described and applied to simulate neutrino spectra that result from dark matter decays. We present first results from our simulations, and highlight some areas that may be of interest for future studies.

Sammendrag

Vi fremfører en prosedyre for å simulere partikkelkaskader med anvendelser innen søk etter mørk materie og neutrinoastronomi. Vi motiveres av de fortløpende utviklingene ved neutrino-observatoriet IceCube, som har gjort tilgjengelig enestående data om den diffuse kosmiske neutrinostrålingen. Vi gjør rede for hvorfor neutrinodata kan bære tegn etter forfall av mørk materie. Vi understreker at forfall av supertung mørk materie generelt kan forventes å utløse høyenergiske partikkelkaskader, som invovlerer både sterke og elektrosvake interaksjoner. Vi bygger på en kaskadeformalisme fra Kvantekromodynamikken for å modelere kaskader av nesten alle partikkler i Standardmodellen. Vi tar også hensyn til forskjellene mellom venstre- og høyrehendte partikler. Det beskrives og anvendes Monte Carlo algoritmer for å simulere neutrinospekterene som resulterer av forfall av mørk materie. Vi presenterer de første resultatene til simulasjonen vår, og understreker noen potensielt interessante retninger for fremtidige undersøkelser.

Acknowledgements

I would like to thank my supervisor, Michael Kachelrieß, for his guidance and consistent availability throughout the past ten months, and in particular during the last weeks. I am very grateful to Lidia Luque, Jonas Lidal, Konstanse Seljelid and Javier de Frutos for taking their time to proofread my work, and providing thorough and insightful feedback. Last, but certainly not least, I want to thank my fellow physics master students, in particular Asbjørn, Konstanse, Jonas, Elise, Tonje, and Michael for their company and moral support, which I have valued immensely.

Contents

Chapter 1

Introduction

For most of history, astronomers had to rely on electromagnetic radiation (visible light, radio waves, gamma rays, etc.), to provide any information on the outer universe. However, recent years are frequently hailed as the beginning of the era of multimessenger astronomy, featuring breakthroughs in the observations of astrophysical phenomena that are independent of electromagnetic interactions. The most notable of these breakthroughs was the discovery of gravitational waves at LIGO in 2016 [, gwaves] allowing the observation of collisions of supermassive objects (black holes and neutron stars) a billion light years away from earth. At the same time, however, the detection of cosmic neutrinos is progressing fast. Following the commissioning of the IceCube detector at the south pole in 2010, a diffuse flux of cosmic neutrinos has been measured for the first time, including detections of the highest-energy neutrinos to date [1].

There are several reasons why the ability to observe cosmic neutrinos is a significant development. In contrast to photons, neutrinos interact rarely with other matter or radiation, allowing them to travel through the universe with little obstruction or attenuation. Despite making the neutrino very hard to detect, this important property is expected to allow physicists (and has to some extent already) to gather information from the most energetic processes of the universe. Much of this information is otherwise obscured by obstacles such as background-light, dust and magnetic fields. One area that has received renewed attention due to the measurements of the IceCube diffuse neutrino flux, is the search for superheavy dark matter (SHDM) [2–5]. Dark matter has been established to contribute to about 25% of the energy in the universe, compared to the 5% that ordinary matter makes up[1] [6]. Yet, the identity of this mysterious form of energy remains unknown. Hopes are that decays of dark matter particles in galactic and extragalactic space produce an overall signal of neutrinos that can be discerned in the IceCube data. Gathering neutrino data is a slow process, as only some tens of cosmic neutrinos can be identified by the IceCube detector every year [1]. As such the IceCube data

[1] For completeness we mention that 70% is thought to be constituted by dark energy, which identity, like dark matter, is unknown, but at least does not behave like matter.

is still rather coarse, even after several years of observations. Nevertheless, the data is already useful in deriving boundaries on viable dark matter models [4].

Very little is known about dark matter, save its strong gravitational effects on the present day universe, as well as its history [6]. However, in the paradigm of quantum field theory (QFT), it makes sense to assume that dark matter consists of massive particles which interact very weakly with ordinary matter. This paradigm suggests a number of natural alterations to the Standard Model (the most accurate description of particle physics to date), in which particles could exist in abundance in the universe [5, 7], despite having evaded experimental detection so far (except by their gravitational effects). The incorporation of dark matter in a quantum field theory normally also implies that the dark matter particles do interact non-gravitationally with standard model particles, albeit very weakly.

We refer to one particular class of dark matter models as heavy, or *superheavy* dark matter (SHDM). This implies that the dark matter particles are several orders of magnitude heavier than the heaviest Standard Model particles. An implication of QFT is that heavy particles that interact with lighter particles will decay into the lighter particles at some rate (that is, with some lifetime). The large mass of the particles itself could provide the high energies that are observed in cosmic neutrinos at the IceCube detector.

Another feature of QFT is the cascading of high-energy particles. Simply speaking, this implies that one very energetic particle is likely to split into a large number of less energetic particles of different types. This is a well-known phenomenon for quarks and gluons, but has been shown to be plausible for other particles as well [8]. This means that the particle spectra produced in SHDM decays could be predictable with basic quantum field theory, without much dependence on the particular dark matter model. In this work, we exploit this fact, and assume only that dark matter is unstable, and interacts with a pair of standard model particles. We then adapt a well-known cascading formalism from quantum chromodynamics (QCD) (that is, the study of the strong interaction) to incorporate electroweak interactions. The probabilistic nature of this QFT formalism invites the application of Monte Carlo techniques to simulate the cascading process. While studies of similar simulations have been conducted in the past, we complement these studies by explicitly modelling the behaviour of all particles of the Standard Model, except for the Higgs particle. We aim to present a simulation scheme that can be applied to and provide insight into the origins of cosmic neutrino flux observed by IceCube.

This thesis is structured as follows; In chapters 2 and 3 we review the status of the research that forms the background for our work. Chapter 2 gives a more thorough account of neutrino astronomy and the IceCube detector, which is the reason for the renewed interest in this area of research. We focus in particular on how the search for dark matter fits into the larger field of neutrino astronomy, as well as the motivations for our work. The capabilities of the IceCube detector are also described here. Chapter 3 contains and overview over the relevant information that is known about dark matter, focusing in particular on SHDM.

In chapter 4 we explain in detail the theoretical framework of our simulation. We start by reviewing the cascading formalism that is known from QCD. This

review forms the basis for the subsequent derivations that we perform in order to extend this formalism. This will culminate in a model of particle cascades that accommodates electroweak interactions, and thus most of the standard model particles. It is also describe how the decay of unstable particles and hadronization of partons can be taken into account in our model.

Chapter 5 describes all practical aspects of simulating particle cascades. We start by explaining the necessary mathematics behind Monte Carlo algorithms. A detailed explanation of how these algorithms are applied in our computer program is provided, using the theory from chapter 4. In chapter 6, we present the first results from our simulations and discuss the insights that may be derived from them. We summarize our findings in chapter 7.

Chapter 2

Neutrino Astronomy

In this chapter, we review the current status of neutrino astronomy. While this is a vast and fast growing discipline, we do not make an exhaustive summary or go into all of the technical details, but aim instead to provide the context of our present investigation. In short, our investigation's objective is to link recent observations by the IceCube neutrino observatory to decays of superheavy dark matter (SHDM), in so far as the latter exists. For completeness, we also summarize the most important alternative explanations for these observations. We will similarly review the status of dark matter research in the next chapter.

2.1 Motivations for Cosmic Neutrino Observation

A crucial property that distinguishes neutrino radiation from more traditional messengers (electromagnetic radiation and cosmic rays) is the weakness of its interactions with other matter. This means that neutrinos can travel distances on the scale of the observable universe essentially unobstructed, despite the matter that is found on its way [9, 10]. In contrast, electromagnetic radiation and cosmic rays are attenuated or blocked completely by matter such as that of the intergalactic medium, gas clouds, and bulk matter (stars, galaxies, etc). Gamma rays (highly energetic electromagnetic radiation or photons) are subject to strong attenuation through interactions with the CMB and extragalactic background light (EBL) over intergalactic distances, especially at energies above $10^2\,\mathrm{GeV} - 10^3\,\mathrm{GeV}$ [1, 11]. The charged nature of cosmic rays means that their trajectories are curved by galactic and extragalactic magnetic fields. In fact, galactic magnetic fields confine cosmic rays with sufficiently low energy to the galaxies in which they are produced (due to the small curvature radii in their trajectories) [12–14]. At the same time, the flux of cosmic rays that are energetic enough to escape their parent galaxies is subject to attenuation by the cosmic microwave background (CMB) on its way to earth. This attenuation becomes significant at extremely high energy (and intergalactic distances), and the cosmic ray flux is generally considered to be strongly suppressed at energies above $5 \times 10^{19}\,\mathrm{eV}$, which is referred to as the Greisen-Zatsepin-Kuzmin

(GZK) limit [1, 12, 15]. Neutrino radiation is not affected by these obstacles, and thus has the potential to provide insight into high-energy astrophysical processes where other messengers do not. This was demonstrated recently when the Blazar TXS 0506+056 was found to be a likely extragalactic source of high-energy neutrino emission. This is providing unprecedented insights into blazar physics, in particular its potential for cosmic ray acceleration [16–19]. In the context of our investigation, it is anticipated that SHDM decays could produce secondary particles in the the range of up to10^{16} GeV (and possibly higher). It thus seems natural that neutrinos may form the least obscured signal of these decays.

Although we will consider SHDM decays in this work, it is more often assumed that the main contribution to the high-energy cosmic neutrino spectrum is made by processes involving the decay of charged pions, which are produced in high-energy collisions of cosmic rays with matter[1] [1, 9, 10, 23] . Charged pions decay to produce neutrinos and muons, the latter of which decay in turn to produce more neutrinos[2] (or anti-neutrinos; we do not distinguish between particles and their antiparticles here, as in most of this work):

$$\pi^{\pm} \;\rightarrow\; \nu_{\mu}\;\mu \qquad\qquad \mu \;\rightarrow\; \nu_{\mu}\;\nu_{e}\;e \tag{2.1}$$

The production of charged pions is accompanied by the production of neutral pions, which decay into a pair of photons [1, 10]

$$\pi^{0} \;\rightarrow\; \gamma\;\gamma. \tag{2.2}$$

Thus, cosmic neutrino spectra are expected to have a predictable gamma ray spectrum as a counterpart [1, 9, 10, 23].

A number of astrophysical objects exist which could plausibly produce an abundance of cosmic rays (highly energetic charged particles such as protons, alpha particles, a few heavier nuclei and electrons) while at the same time providing the necessary interaction sites for pion production, for example starburst galaxies, active galactic nuclei (AGNs), and blazars, to name just a few [17, 18, 23]. Interactions between cosmic rays and the photons of the ELB and CMB in intergalactic space are also expected to result in a measurable flux of high-energy neutrinos (since this is the same effect that causes the GZK limit energy, see above, these neutrinos could provide insight into the existence of cosmic rays beyond that energy). Yet, the origins of both cosmic rays and cosmic neutrinos have in general not been confirmed [1, 9, 23, 24]. Profound insights could therefore be provided into the highest-energy processes of the universe if correlations between observations of neutrinos and those of cosmic rays could be established. This has traditionally been the primary motivation for cosmic neutrino observation [1, 9, 24].

In recent years though, there has been a revived interest in superheavy dark matter, i.e. the notion that dark matter may exist as particles with masses that are

[1] Nuclear reactions in stars and supernovae also come to mind as production mechanisms of neutrinos, however these typically don't produce neutrinos with energies of order higher than some tens of MeV [20–22], while we are interested in neutrinos of at least 10^{4} GeV in our work.

[2] The presented decay channels are implicitly the predominant ones, though not technically the only ones.

several orders of magnitude above the weak scale ($\sim 10^2$ GeV). Dark matter masses of up to 10^{16} GeV are considered [4, 5]. This idea is particularly enticing because it could provide an alternative source of cosmic rays other than the class of scenarios described above, for which purpose it was orignially conceived [2, 3, 5, 25]. While SHDM particles should have low kinetic energy, their large masses could provide the energy that is ultimately attained by standard model particles such as cosmic rays and neutrinos, which are received as signals on Earth. How this transfer of energy would occur is subject to a wide variety of different models. However, it is reasonable to assume that most scenarios will ultimately involve the production of high-energy neutrinos. One reason for this is that for particles with masses above 10^6 GeV, any decay or annihilation is likely to produce a *particle cascade* [8], which we will discuss in detail in chapter 4. Loosely speaking, this means that any primary decay into standard model particles will set off a chain reaction of standard model interactions, thus producing particles of all types, whereof a large share may be neutrinos. While in some scenarios, cascade products may be dominated by gluons and quarks (partons), these will ultimately also produce a neutrino spectrum, as partons hadronize into pions which decay into neutrinos as discussed above.

In addition to the cascading argument, many SHDM models consider decay of dark matter directly into neutrinos (collectively referred to as the neutrino portal paradigm) [26–28]. In a very roundabout sense, a prevalent motivation behind this is the fact that a full description of neutrino physics is all but guaranteed to require theories that reach beyond the standard model. One important indication of this is that the standard model strongly suggests that neutrinos either have no mass, or a mass similar to that of other standard model particles; nevertheless experimental evidence shows conclusively that neutrinos are indeed massive[3], but these masses are too small to measure (so far). [29]. It is thus natural to anticipate models that explain both the identity of dark matter as well as the neutrino's tension with the standard model at the same time. Particularly common are models which couple dark matter to a hypothetical right-handed (or sterile) neutrino, which in turn mixes with the ordinary left-handed neutrino (that is, the two can transform into each other at some rate). In addition to some relative mathematical simplicity, this model is convenient because the existence of the right-handed neutrino would simultaneously explain the smallness of the ordinary neutrinos' masses [26–28, 30].

In summary, cosmic neutrino observations lay crucial groundwork for viability tests of many dark matter models. In the present work, we aim to study in particular the aforementioned cascading process that is implied in most scenarios of SHDM decay. We will focus in particular on a scenario where dark matter particles decay at tree level into two neutrinos:

$$X \;\rightarrow\; \nu\,\nu, \tag{2.3}$$

where X denotes the dark matter particle. The implications of this are in principle only that the decay of SHDM is bound to produce an (intermediate) pair of neutrinos with energies equal to half the mass of X, and is as such quite non-restrictive.

[3] It is worth pointing out that this discovery is also a result of neutrino astronomy, although with a focus on solar and supernova neutrinos

We note that there is no immediate reason why dark matter particles should not be able to decay equally well into other SM particles, and so we will consider other decay channels in our work as well.

2.2 The IceCube Neutrino Detector

The IceCube telescope at the south pole is the largest and most sensitive detector of astrophysical neutrinos, being the first kilometer-scale neutrino detector of its kind [10]. It is also the detector that has measured the highest-energy neutrinos to date, having reported the first observations of neutrinos with energies at the PeV-level [31, 32]. In principle, IceCube should be able to detect neutrinos with energies over 10^3 PeV [33]. Several years of IceCube observations have made available the first experimental values of a diffuse cosmic neutrino flux between 10 TeV and 10 PeV. This has sparked renewed interest in the search for super heavy dark matter in our galaxy and beyond. We summarize here the most important features of the IceCube detector as well as the status of its observations.

2.2.1 Purpose and Function

Since neutrinos interact so rarely with other matter, neutrino telescopes are made as large as possible to increase the probability of interaction. In addition, larger sizes improve the chance that the signals produced by such interactions are completely contained in the detector, making more precise measurements of energy and incident direction possible. The IceCube telescope achieves an effective volume of a cubic kilometer by exploiting naturally occurring glacier ice at the south pole as the detecting medium. An array of 5160 optical modules containing photomultipliers have been lowered into the ice via drilled holes (see figure 2.1) in order to record the signals produced by neutrino-ice interactions [1, 10, 33].

When neutrinos pass through the Antarctic ice, they may (with some small probability) interact with the ice's nuclei in one of two ways, referred to as charged current interactions and neutral current interactions [1, 10, 34]. Charged current interactions produce electrons, tau leptons or muons, the latter of which continue to travel through the ice in roughly the same direction as the incident neutrino. Charged particles which travel through a dielectric medium (such as ice) at speeds higher than the speed of light in that medium produce light signals via the Cherenkov effekt, which is collected by the photomultipliers. The total energy delivered to the photomultipliers determines the lower bound on the incident energy, and the incident neutrino's energy is estimated by taking the median of a theoretical distribution that takes into account energy transfer to the nuclei in the ice [1, 34]. The shapes of these signals allow for a determination of the neutrinos' incident directions and flavour (see figure 2.2). Muon-neutrinos are the easiest to identify and trace, because the muons that they produce mostly travel through the detector unimpeded. This produces a Cherenkov signal that spreads out evenly from the particle's trajectory (forming an expanding cone of light) that is relatively easy to identify. Electron- and tau-neutrinos on the other hand produce

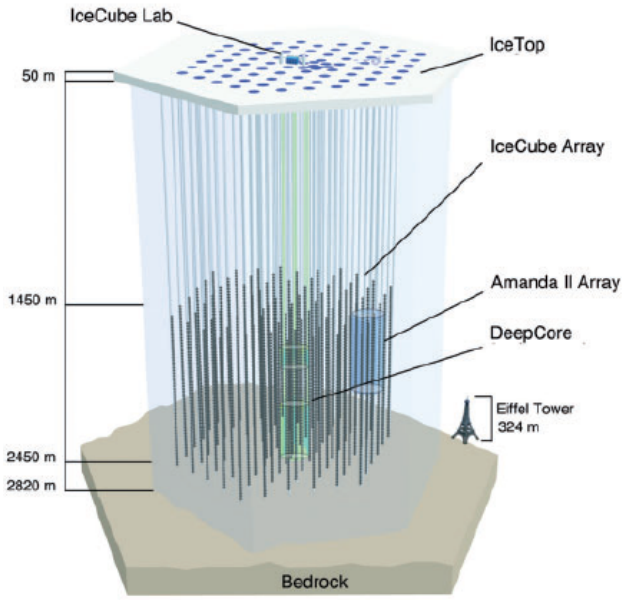

Figure 2.1: Visualisation of the IceCube detector, reproduced from [1].

electrons and tau leptons, which scatter on the ice molecules, creating a roughly spherical signal [1, 34]. Neutral current interactions on the other hand produce hadronic cascades for all three neutrino flavours, which also produce spherical signals due to scattering. These are difficult to distinguish from the charged current interactions of electron- and tau-neutrinos. Hence, charged current interactions of muons deliver the only signals for which the neutrino flavour can be easily identified. Determination of the incident direction for cascading events is possible within an uncertainty of up to 15° for all cases, although developing reconstruction techniques are expected to improve this uncertainty to a few degrees in the future. The incident direction of track-like events from muon neutrinos can on the other hand be determined to within less than 0.4° [1].

IceCube observations are subject to a huge number of background particles. Atmospheric neutrinos and muons are produced when cosmic rays interact with nuclei in the atmosphere and the relevant cosmic neutrino detections must be isolated from these[4]. One way to eliminate the muonic background is to record exclusively those signals that are incident from the northern hemisphere; neutrinos can pass through the Earth unobstructed (although with some absorption), while muons are absorbed fully by the Earth. Thus, muons that pass through the detector from the direction of the northern hemisphere can be assumed to have been produced by neutrinos reacting inside the earth, close to the detector. This

[4]The rate of muon interactions with the detector is about 3000 a second, while neutrino interactions happen at a rate of 100,000 a year. Thereof, some tens are of cosmic origin, while the rest are atmospheric [1].

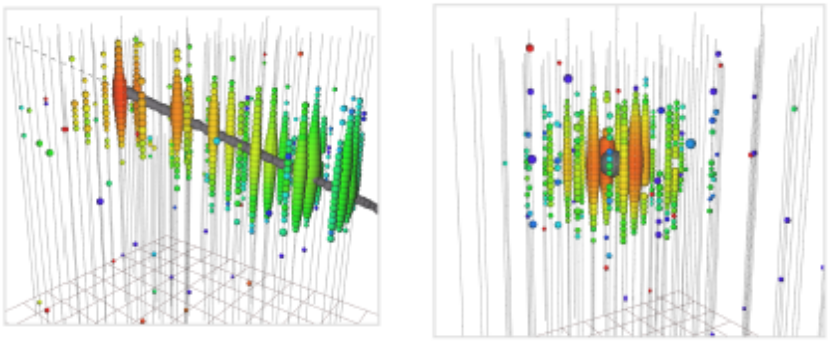

(a) (b)

Figure 2.2: Visualizations of the two common kinds of signals in IceCube, reproduced from ref. [35]. Tracks (a) occur when muons pass through the ice, emitting Cherenkov light from its trajectory. Spherical cascades (b) occur when electrons or tau leptons (or their decay products) scatter on the ice molecules.

effectively increases the detector size, and improves determination of the neutrino's incident direction, as more of the tracks extend over the full length of the detector [1]. On the other hand, detections are in these cases restricted to muon-neutrinos, and the incident energy cannot be determined as accurately, due to an unknown amount of energy being deposited outside the detector [1]. Cosmic ray muons can be excluded from both northern- and southern sky observations by designating the outer rim of the detector as a veto area, and including only those signals that start somewhere within the rest of the detector (muons arriving from outside the detector will naturally produce tracks starting at the outer rim). This improves energy measurements (possible to within 10 %-15 %), but makes determination of the incident direction less accurate [1].

In order to determine which neutrinos are of cosmic origin (as opposed to atmospheric), the degree to which neutrino events coincide with muon detections are considered. Since atmospheric neutrinos are produced together with muons in the atmosphere, missing muon signatures during a neutrino event imply that it is unlikely that the neutrino is of cosmic origin [1, 33]. In addition, a shower array (IceTop) is installed above the neutrino detector, which is able to detect the atmospheric showers in which an atmospheric neutrino is produced [36]. Furthermore, the flux of atmospheric neutrinos are easier to model theoretically than cosmic neutrinos, and it is found that a vanishing number of atmospheric neutrinos are expected above an energy of 10^5 GeV, leaving only a cosmic origin for detections above this threshold [1, 10, 33].

2.2.2 Current Status of Observations

Several years of IceCube observations have accumulated to a first look at the diffuse neutrino spectrum between 10^3 GeV and 10^7 GeV. This has motivated many stud-

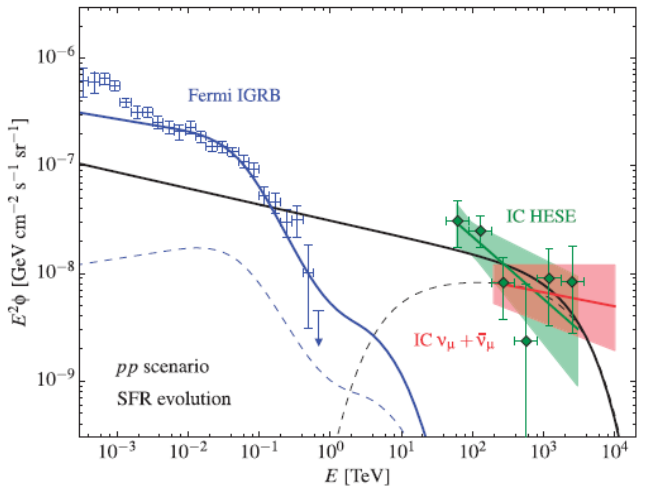

Figure 2.3: Visualization of IceCube cosmic neutrino data (green crosses) from 4 years of observation, reproduced from ref. [1]. Solid lines depict various models of neutrinos and gamma ray fluxes. In particular, the green line and shaded area represent a power-law fit for the neutrino spectrum. The blue line represents a model for the gamma ray flux related to decaying cosmic ray pions and cascading on background light; the black line represents the model for the corresponding neutrino production.

ies into the plausible origins of this flux, amongst which is the decay of superheavy dark matter.

A central question in determining the source of the high-energy neutrino flux is to which extent the latter originates in or outside the Milky Way; the dark matter decay model implies that the dominating component of the flux must be of galactic origin. One main indicator of this is whether the neutrino flux is accompanied by a compatible gamma-ray flux. As explained section 2.1, gamma rays are produced whenever high-energy neutrinos are (and with a similar spectrum) if the latter are produced via pion decay. A dark matter-induced cascade would naturally also produce a spectrum of gamma rays, along with the neutrinos. However, gamma rays are strongly attenuated when travelling extragalactic distances. Hence, the lack of a compatible gamma ray signature would suggest that the neutrino signature is predominantly produced in far-off galaxies. While no gamma ray flux data is available in the 10^3 GeV to 10^7 GeV range, a gamma ray flux in the range 1 GeV to 10^3 GeV has been observed that could be the result of higher-energy gamma rays being attenuated by interactions with the CMB and ELB. It has been shown [1, 37] that this flux is in part compatible with the scenario where extragalactic gamma rays are produced together with the observed neutrinos in hadronic processes (for example cosmic ray interactions with atomic matter, see section 2.1).

Yet, there is evidence for a galactic contribution to the neutrino and gamma

ray spectra. Roughly speaking, the neutrino spectrum observed for energies above 10^3 GeV plausibly represents a continuation of the gamma ray spectrum observed below the same energy [38, 39]. The second indication of Galactic contributions is an apparent anisotropy in the flux above 10^5 GeV, that is, a somewhat harder flux [40] from the direction of the Galactic plane than at higher galactic latitudes. This would be expected in the SHDM scenario, seeing as the dark matter halo, as seen from Earth, appears thickest in the direction of the galactic plane.

The neutrino spectrum also gives some reason to consider the existence of a source other than the conventional hadronic processes followed by pion decay. The authors of [39] find that the high-latitude galactic gamma ray flux is only compatible with the neutrino flux if the former shows significant spectral hardening around 300 GeV. As the conventional sources do not exhibit this behaviour, a so far unknown production mechanism is required. Similarly, the authors of [1] report that the spectrum in the range 3×10^4 GeV to 10^5 GeV cannot be explained by a single power-law fit, and suggest therefore a second significant source of neutrinos in this range.

Chapter 3

Dark Matter

In this chapter we go through some of the important features of dark matter research. As in the last chapter, we do not intend to review the whole topic in great detail. Instead we aim to give the reader some background that will put the premise of our investigation into context of current research. That premise is that the universe is filled with super heavy dark matter particles, which in decaying produce a neutrino signal that can be detected by neutrino telescopes such as IceCube.

3.1 Distribution at the Galactic Level

The notion of dark matter was first conceived of because the velocities of galaxies in galaxy clusters – and later those of stars in in galaxies – were larger than expected [41]. The masses of stars are related to their luminosities, and so the masses of galaxies can be estimated by measuring their brightness. However, the galaxy and cluster masses that are estimated in this way are too low to gravitationally bind the stars and galaxies in them (at least at their particular orbital distances), given their measured velocities (which can be measured by spectral Doppler shifts). In particular, galactic rotation curves (plots of stars' orbital velocity around the galaxy as a function of distance r from the center) are expected to decrease as $\frac{1}{\sqrt{r}}$ at large distances, but instead remain quite flat [42]. Observations of stellar dynamics, in the particular fitting of dark matter models to rotation curves, are still used to investigate the dark matter distributions of the Milky Way.

We note that there exists a wealth of other evidence for the existence of dark matter, including gravitational lensing effects, considerations of galaxy formation and the universe's evolution, as well as observations of the "Bullet cluster". It has been proposed that gravitational dynamics could be modified on astronomical scales, in order to eliminate the need for dark matter. Such models have however been experimentally unsuccessful, and observations of the Bullet cluster make a compelling case for dark matter independent of the gravitational force law [43]. See for example [41] for a review on the history and evidence for dark matter.

Computer simulations of galaxy formation predict how the dark matter density

varies with distance from the galactic center. It is found that galaxies are surrounded by a halo of dark matter with a radius that can be significantly larger than that of the galactic disc. The halo is not flat like the galactic disc, because the weakness of dark matter interactions implies that transverse velocity components are not cancelled by friction forces during halo-formation, as they do for ordinary matter during galaxy formation. One of the most commonly applied profiles of the dark matter density $\rho(r)$ with distance r from the galactic center, is the Navarro-Frenk-White (NFW) profile [44]:

$$\frac{\rho(r)}{\rho_{\text{crit}}} = \frac{\delta_c}{\frac{r}{r_s}\left(1+\frac{r}{r_s}\right)^2} \tag{3.1}$$

Here, $\rho_{\text{crit}} \sim 10^{-5}\,\text{GeV}\,\text{cm}^{-3}$ is for all practical purposes the large-scale energy density of the universe. The parameters δ_c and r_s are specific to the galaxy. The scale length r_s gives a notion of the radius of the dark matter halo, as the dark matter density becomes of the order of the critical density at this radius. In the case of the Milky Way, the scale radius is found to be $10-40\,\text{kpc}$ [45]. For comparison, the Earth's position is at a radius of around $8\,\text{kpc}$, where the dark matter density is about $0.4\,\text{GeV}\,\text{cm}^{-3}$.

While the density profile diverges at low r, indicating limitations in the model, it predicts that the dark matter density increases sharply close to the Galactic center, which observations support [46]. This implies, that if dark matter does emit an observable signal, this should be stronger towards the Galactic center. While dark matter is not expected to have significant overdensities in the Galactic disc (that is, it is approximately spherically symmetric), the signal strength is still expected to be stronger from the direction of low galactic latitudes as opposed to high ones. This is because of Earth's off-center position in the galactic disc, which causes us to see more of the dark matter halo in those directions. While IceCube observations are not yet substantial enough to test these simple predictions, some indications have been found that the observed neutrino flux is indeed more pronounced from the disc (see section 2.2.2).

3.2 Super Heavy Dark Matter, and Other Candidates

In our following investigation, we will consider the possibility that dark matter exists in the form of particles with masses above $1\,\text{PeV} = 10^6\,\text{GeV}$. However, it is worth noting that other dark matter candidates are more commonly studied. Some favoured candidates include:

- **The WIMP (Weakly Interacting Massive Particles) model.** This paints a rather natural picture, in which dark matter does interact with standard model particles via the known weak interaction (or some novel weaker interaction) [7, 47, 48]. This implies that in the early and hot universe, random annihilation and creation of dark matter via interactions with standard

model particles was commonplace, i.e. dark matter was in chemical equilibrium with the rest of the universe. Since the probability of interactions decreases with decreasing temperature, and the dark matter is diluted due to the expansion of the universe, interactions rates have become negligible over time. Since the interaction cross-section typically goes like $1/m_X^2$ (with m_X being the dark matter mass), this is more so the case for dark matter particles than ordinary ones if m_X is significantly larger than the largest masses of standard model particles (which are of order 10^2 GeV). A commonly considered candidate for WIMP-type particles is the neutralino, which arises naturally in the theory of supersymmetry, which simultaneously serves to explain a range of other mysteries of particle physics [49].

- **The axion model.** The axion model suggests that dark matter consist of very light particles called axions. These have the advantage of also solving the strong CP problem (the fact that strong interactions seem to obey CP symmetry, even though conventional QCD suggests that they should not), for which they were originally hypothesized [50].

- **Sterile neutrinos.** Also referred to as right-handed neutrinos, these are a natural extensions to the standard model's theory of neutrinos, which only includes a left-handed neutrino (in practice meaning that the neutrino's spin is always measured to be parallel with its momentum, never anti-parallel). The existence of the sterile neutrino could simultaneously explain the identity of dark matter and why experiments find the neutrino to have a very small mass, despite the standard model's prediction that neutrinos should be massless [29, 30, 51].

While the above constitute favoured versions of dark matter, we must consider a different kind of candidate in this work. This is because we are interested in dark matter particles with masses above 10^6 GeV, so that they can provide the high energies of the neutrinos which are observed by the IceCube telescope (see section 2.1). Neither of the candidates listed above are compatible with masses of these magnitudes. Axions and sterile neutrinos are expected to have masses of the orders of eV [50] and keV [51] respectively. The WIMP paradigm is less restrictive, but strongly disfavors masses beyond the order of 10^5 GeV. Masses above this scale would render WIMP annihilation cross sections too small, in the sense that too few WIMPS would annihilate until the present day, leaving more dark matter than what is compatible with observations [7, 47].

The existence of superheavy dark matter is however considered to be a natural consequence of many models of the universe's evolution [5, 47]. In particular, production of superheavy particles seems likely in the end stages of inflation [7] – the period of extremely rapid expansion straight after the big bang [6]. From a QFT perspective, inflation is generally assumed to be driven by a particle field (referred to as the inflaton), in which resides the energy density that causes space to expand. Conversely, the expansion of space causes the inflaton field to evolve. At the end of inflation, the inflaton field is able to interact with other particle fields, thus passing on its energy to these, leading to the creation of particles (this

process is referred to as *reheating*) [5, 7, 52, 53]. If the inflaton can interact directly with the dark matter field[1], then the presence of dark matter does not first require that dark matter be in equilibrium with the rest of the universe at some point after reheating. Hence, the dark matter mass can be much larger than in WIMP models, presumably up to 10^{15} GeV [5].

In a similar type of model, dark matter is created as a more direct consequence of the expansion of space during and at the end of inflation. This is based on the knowledge that certain particles can be produced by variations in the rate of expansion of space [54, 55]. Alternatively, this gravitational production can be viewed as an interaction between dark matter and the inflaton (which is still considered to be the original reservoir of energy) via an intermediate graviton [55–57]. This paradigm is non-restrictive, and thus attractive, in the sense that it requires few assumptions. Dark matter interacts with gravity by definition, and inflation is well-supported by observations [6]. This all but guarantees the gravitational production of dark matter particles in the early universe, that is, given that the dark matter field exists in the first place. However, for this to be the dominant production mechanism, and for observational data to hold, the dark matter mass has to be of the order of the inflaton mass (which has been constrained to about 10^{13} GeV) [5, 7, 47, 57]. In addition, this model opens the possibility that dark matter does not interact at all, which would make it very problematic to gain further insights into its nature.

Another paradigm of dark matter production provided by quantum field theory is the decay of topological defects. Loosely speaking[2], a particle field tends to behave in a way that minimizes some potential energy. That potential energy may have several minima, and space could be divided into regions which correspond to different minima, because of phase transitions in the early universe (during inflation [5]). The way this happens is that, as the universe cools, the number of minima changes from one to two (or several), and the particle field thus "falls" into either of these new minima randomly and at arbitrary points in space. From those points, the field at neighbouring points fall into the same minima, creating expanding regions where the field corresponds to the same minima. However, where these regions corresponding to different minima meet, the field is forced to take on a large amount of energy. This is because the field must be continuous, and values between two minima of the potential energy naturally corresponds to a large potential energy. This energy can be released though, as one minimum gradually takes over all of space, causing the defect to decay. The released energy can give rise to energetic particles, such as superheavy dark matter. The takeaway is that energy could be stored in topological defects from the time of inflation until potentially the present day, producing superheavy particles that need never have been in equilibrium with anything else. This paradigm thus allows for an easing

[1] By *directly* we mean that the production of a dark matter particle doesn't first require an intermediate interaction with another particle of the standard model; intermediate interactions with other exotic bosons are however common in reheating models.

[2] Indeed, we only attempt to give an intuitive notion of topological defects here, which is in reality a particularly profound topic, in order to distinguish it from the other mechanisms of dark matter production. For a more detailed review, we refer to [58].

of the constraints that are typically put on the masses and lifetimes of superheavy dark matter. Evidence for cosmic topological defects has yet to be observed though.

We will not go deeper into the origins and properties of dark matter in this work. For the following investigation, it suffices to know that it is theoretically sound to consider the existence of dark matter particles with masses between 10^6 GeV and 10^{16} GeV, and which decay into pairs of standard model particles (as discussed in section 2.1).

Chapter 4

Modeling particle cascades

In this chapter, we describe a model of particle cascades which can be used to predict the spectrum of particles that are produced by the decays of superheavy dark matter (SHDM). From an observational perspective, a cascade only entails the appearance of a large number of particles following the decay of some heavy particle (or by the collision of two energetic particles). In other words, only the final particles that are ultimately produced in the cascade can be observed, not the "process" by which this occurs. However, from a theoretical standpoint, a cascade can be described as a sequence of sub-processes: the original particle splits into two new (virtual) particles, which in turn split into four, and so on. Given that each splitting happens with a certain probability, the cascade can be modelled as a random process, and hence simulated using Monte Carlo methods. This chapter is devoted to determining suitable expressions for these splitting probabilities, which form the groundwork of our simulation of particle cascades – how we apply the theory in practice is explained in chapter 5.

We begin by looking at the special case of parton cascades, that is, cascades involving only quarks and gluons, the formalism of which is known from quantum chromodynamics (QCD). We will then adapt this formalism to the electroweak sector of particle-interactions, so that we may apply it to the other particles of the standard model (except the Higgs particle). We also describe simple models of how the final particles from the cascades decay and hadronize.

4.1 Parton Cascades

By a parton cascade, we mean one where particles interact only via the strong interaction; whenever a particle splits, at least one of the incoming or outgoing particles is a gluon (commonly referred to as the force carrier of the strong interaction); one or two of the other particles may be quarks. We discuss under which conditions these cascades occur, and illustrate how to break them down into a sequence of comprehensible steps that are suitable for simulation.

4.1.1 Conditions for Parton Cascades

As indicated above, a parton cascade can be modelled in terms of a sequence of splittings, each of which happens with a certain probability. This probability is proportional to the strong coupling α_s, which is dependent on the energy scales involved in the splitting (for an in-depth review on the strong coupling, and explicit expressions, see for example [59]). To be more precise, we say that the coupling is a function of the momentum flow k^2 in the interaction (where k^μ denotes the four-momentum of the particle that splits). In particular, the coupling decreases with increasing k^2. Since the coupling in general determines the strength of strong interactions, below a certain value of k^2, α_s is greater than the order of unity, and interactions between partons become so strong that they coalesce to form hadrons (e.g. nucleons and pions). This value of k^2 is denoted by Λ^2_{QCD}, where $\Lambda_{QCD} \approx 0.250\,\text{GeV}$ is referred to as the QCD scale (or strong scale). When particles are bound in hadrons, they cannot start cascades, and we thus have the first condition for cascades to occur:

$$t = k^2 \overset{!}{>} \Lambda^2_{QCD} = 0.250\,\text{GeV}. \tag{4.1}$$

On the left-hand side, we have indicated for completeness that the momentum flow k^2 is for our purposes equal to the virtuality t (which we will introduce later), by which we will refer to it throughout most of the rest of this text.

While large momentum flows prevent partons from being bound in hadrons, they also imply that the strong coupling, and thus the probability of splitting is relatively low. Intuitively, this would mean that cascades, which imply the occurrence of a large number of consecutive splittings, are rather unlikely. However, quantum field theory (QFT) dictates that the probability of a splitting which consists of a gluon being emitted by a quark or another gluon is proportional to a factor

$$\frac{1}{\left[(p+q)-m^2\right]^2} \to \frac{1}{\left[2p\cdot q\right]^2} \sim \frac{1}{E^2\omega^2\left(1-\cos\theta\right)^2}, \tag{4.2}$$

The arrow indicates the relativistic limit, which we will also assume throughout this work, seeing that we are interested in highly-energetic particles. The pronumerals p and q denote the four-momenta of the outgoing particles, m and E the mass and energy of the emitting particle (in the final state), ω the energy of the emitted particle, and θ the emission angle. This means that despite the relative weakness of the coupling, the emission probability becomes large for *soft* and *collinear* emission (referring to gluons that are emitted with low energy or at low angles respectively). This implies the next limit that we will consider consistently, namely small emission angles (the softness condition does not immediately imply any simplifications to later calculations):

$$\theta \overset{!}{\ll} 1. \tag{4.3}$$

The factor (4.2) diverges in the limits $\omega \to 0$ and $\theta \to 0$, collectively referred to as infrared (IR) divergences. These make the splitting probability seem unphysical at a first glance. However, in reality, this factor only represents a first approximation to the physical splitting probability, and the divergences disappear when

taking into account corrections due to the exchange of virtual gluons between the two outgoing particles [60]. In the calculations that follow later, we avoid the divergences because the model implies natural cut-offs on the valid range of ω and θ (which we we will incidentally express in terms of other variables).

Lastly, analytical calculations show that in the soft and collinear limits, factors of the form $\ln^2(k^2/m_q^2)$ dominate the splitting probabilities [60], where m_q denotes the mass of the quark that is involved in the spliting (if any). These imply a separate cascading condition for quarks with $m_q > \Lambda_{QCD}$, namely[1]

$$t = k^2 \overset{!}{\gg} m_q^2, \tag{4.4}$$

which incidentally confirms that we can assume the relativistic limit in our calculations.

With the knowledge of these conditions in hand, we proceed to the explicit calculations of splitting probabilities.

4.1.2 General Strategy

Our overarching goal is to predict the spectrum of particles, that is, the types and energies of particles that are produced in a cascade following the decay of some heavy (dark matter) particle. This essentially means that we have to find the probability that a certain type of particle with a certain energy is produced in any given cascade. Basic QFT allows us to find a related quantity, namely the probability of a specific realisation of a cascade (for example the one in figure 4.1a or the one in 4.1b) to occur. In other words, the probability that the exact sequence of splittings indicated by either figure occurs after a decay can be found using the Feynman rules (which we go into later in section 4.1.3). If we could find the probabilities of every thinkable sequence of splittings to occur, these would directly imply the probabilities for specific particles (with specific energies) to be produced, and hence the cascade spectrum.

Clearly, this approach of finding the decay spectrum is impossible, not only because a cascade in principle could consist of an infinite number of splittings, but in particular because every splitting can divide the parent particle's momentum in an infinite number of ways. Nevertheless, it is this approach that we will in essence try to simulate. To be specific, we will express the probability of a specific sequence of splittings (for example the one in figure 4.1b) to occur given that an identical sequence, except with one less splitting (figure 4.1a) has already occurred. We will find that this probability does not depend on the previous history of the cascade, but only on the parent particle and it's momentum. Hence it is in principle simple to simulate the cascades in a computer program, by splitting particles successively and randomly, according to the probability distributions that we find. We should obtain as spectrum similar to the theoretical cascade spectrum by adding the final particles of a large number of thus simulated cascades.

[1] Throughout this chapter and this work, we impose the natural units, $\hbar = c = 1$, implying equivalence between mass, energy and momentum.

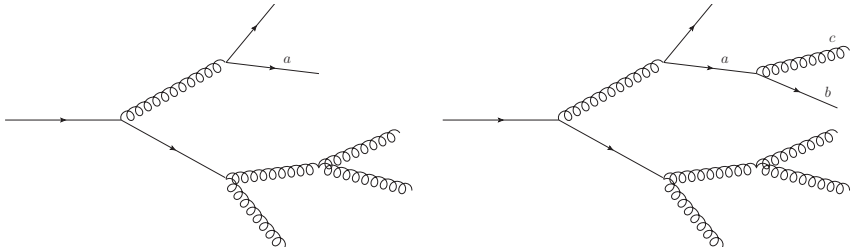

(a) (b)

Figure 4.1: Visualization of the Feynman diagrams of two parton cascades. Straight lines represent quarks and curly lines represent gluons. The first quark is implied to be one of a pair that is produced in a heavy-particle decay. The cascades in a and b are identical, except that the quark denoted by a undergoes a splitting in b. Given that all the involved momenta are otherwise identical between the two cascades, the probability for the cascade in b to happen is the same as for the one in a except for one factor that is contributed by the extra vertex between particles a, b and c, and a's promotion to an internal line. This extra factor may be viewed as the probability of splitting of particle a.

It is worth pointing out again, that the successive splittings that we are talking about are not physically observable, and are arguably only a common mathematical trick from QFT that has been established to yield physical final results. The notion that certain splittings happen before or after others only serves the flow of our explanations, but does not imply that the cascade actually represents a sequence of splittings that is ordered in time. The entire cascade is for all practical purposes immediate. We thus also refer (as usual) to the intermediate particles as *virtual* (or *off-shell*), as they do not represent physical particles.

As a simplifying approximation, we restrict ourselves to those Feynman diagrams in which particles only split, rather than recombining from time to time. In other words, the process consists of a combination of tree-level splittings such as the one in figure 4.2. In such a splitting, an initial particle a splits into two particles b and c. The defining parameters of the splitting are the angles θ_b and θ_c at which b and c are respectively emitted, and the virtuality t_a of particle a. Virtuality is for a general particle i defined as $t_i \equiv k_i^2 - m_i^2$, where k_i^μ and m_i are the particle's four-momentum and mass respectively. It is thus a measure of how off-shell the particle is (as for a physical particle, k^2 is necessarily equal to m^2). In the relativistic approximation $k^2 \gg m_i^2$, and virtuality becomes equal to the momentum flow,

$$t_i \simeq k_i^2.$$

In addition to these parameters, the fraction of a's energy E_a that is passed on to b is important, an naturally the fraction that is passed on to c is as well. We

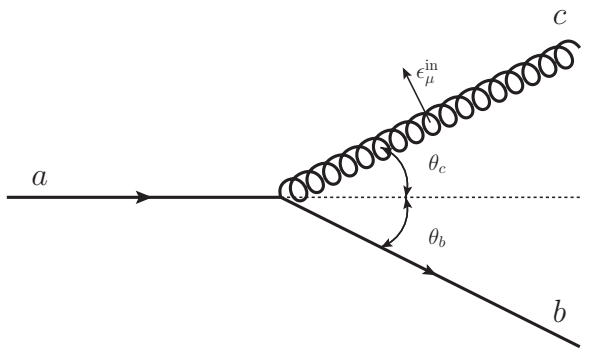

Figure 4.2: Visualization of a splitting starting from a quark a and producing another quark b and a gluon c. Particles a and b are emitted at angles θ_b and θ_c with respect to particle a's momentum, which in general are not equal. The direction of the gluon's polarization vector parallel to the plane of the momenta, ϵ_μ^{in}, is indicated. It is implied that there is also a component $\epsilon_\mu^{\text{out}}$ transverse to the plane of the paper. It is assumed that this process happens as part of a cascade, such as the one visualized in figure 4.1b.

denote these by z and $1-z$ respectively:

$$z = \frac{E_b}{E_a} \qquad\qquad 1 - z = \frac{E_c}{E_a} \tag{4.5}$$

The parameters t_a, θ_b, θ_c, and z are not independent, and each splitting is for our purposes sufficiently parametrized by two of them.

Consider now the Feynman diagram of some (incomplete) cascade, and denote the corresponding probability amplitude[2] by A_n, where the index n denotes the total number of splittings that have occurred so far. Assume then that one of the particles at the end of that cascade splits; then the new Feynman diagram will be the same as the old one, but with one extra vertex and internal line, as well as two new external lines (this is illustrated, for example, by the transition from figure 4.1a to 4.1b). According to the Feynman rules, the new probability amplitude will be $A_{n+1} = (V/t)A_n$, where t is the virtuality of the particle that has split. The factor $1/t$ corresponds to the extra internal line (commonly referred to as a propagator), and V corresponds to the extra vertex (in the case of figure 4.2 this is a fermion-gluon-fermion vertex). Hence,

$$|A_{n+1}|^2 = \frac{|V|^2}{t^2}|A_n|^2 \tag{4.6}$$

[2] As opposed to the probability, which is by definition given by $|A_n|^2$

We can thus show (as we will do below) that that the probability for the last splitting to happen, given the first n splittings, can be expressed as [3]

$$\frac{\mathrm{d}\sigma_{n+1}}{\mathrm{d}\sigma_n} = \frac{\mathrm{d}t}{t}\mathrm{d}z\frac{\alpha_s}{2\pi}P(z), \tag{4.7}$$

where $\alpha_s \equiv g_s^2/(4\pi)$, and g_s is the QCD coupling constant[4]. The function $P(z)$ is referred to as a *splitting function*, and depends only on z, but has a different form depending on the splitting vertex V. It is worth mentioning that the factor $\frac{1}{t}$ at first sight implies that the splitting probability is suppressed at large virtualities, thus making cascading less likely. However, this suppression is compensated for at small values of z, as the splitting functions typically contain factors of $\frac{1}{z}$ and $\frac{1}{1-z}$, which correspond to soft divergences.

In what follows, we will show that equation (4.7) is indeed true, referring to the case in which a quark emits a gluon as in figure 4.2 to keep the discussion concrete. The most important take-away will be that we will find the explicit form of the splitting function $P(z)$ in the process. Afterwards, we will also find the splitting functions for the remaining cases, though only providing the details that set their derivation apart from that of the first case. These derivations are crucial to this work, as they will help us determine a similar formalism for electroweak cascading in section 4.3.

4.1.3 Derivation of Splitting Probabilities

The Feynman amplitude corresponding to the quark-quark-gluon vertex is [61]

$$i\ g_s\ T^a_{ij}\ \gamma^\mu,$$

where γ^μ denotes the well-known gamma-matrices (or Dirac matrices). The scalar T^a_{ij} is the element (i,j) of the a^{th} generator of the $SU(3)$-algebra (see for example ref. [61]). Physically, a indicates the type of gluon that is emitted (thus spanning the values 1,2,...,8), while the indices i and j indicate the colors of the two quarks (thus spanning the values 1,2 and 3). These distinctions are however undetectable, so the indices will simply be summed over later on (equation (4.19)).

According to conventional perturbation theory, the probability amplitude of the splitting now becomes[5]

$$V_{qqg} \ = \ i\ g_s\ T^a_{ij}\ \bar{u}^{\text{out}}_H\ \epsilon^*_\mu\ \gamma^\mu\ u^{\text{in}}_h \tag{4.8}$$

Here, ϵ^*_μ is the complex-conjugated polarization vector of the outgoing gluon. The column-vector u^{in}_h is the Dirac spinor corresponding to the incoming fermion. The

[3] We express the probability as a ratio of cross sections, which is the same as the ratio between the probability of the cascade to happen with only the first n splittings and for it to happen with the extra splitting. It is useful to express the splitting probability in terms of cross sections, as this allows a direct connection to Feynman amplitudes.

[4] The term *coupling constant* is used interchangeably for α_s and g_s. The latter is used more commonly when talking about Feynman amplitudes, rather than physical probabilities or cross-sections

[5] We use the Einstein summation convention.

row-vector[6] $\bar{u}_H^{\text{out}} \equiv u_H^{out,\dagger}\gamma^0$ is the Dirac conjugate of the outgoing Dirac spinor. The indices h and H denote the chiralities (left or right) of the respective fermions. In the relativistic limit, right- and left-handed Fermions don't mix, and we will essentially treat them as separate particles throughout this chapter.

The explicit forms of the dirac spinors, in terms of a particle's emission angle θ and energy E are given as follows[7]:

$$u_{\text{L}} = \sqrt{E+m}\begin{pmatrix} -\sin\frac{\theta}{2} \\ e^{i\phi}\cos\frac{\theta}{2} \\ \frac{|\overrightarrow{p}|}{E+m}\sin\frac{\theta}{2} \\ -\frac{|\overrightarrow{p}|}{E+m}e^{i\phi}\cos\frac{\theta}{2} \end{pmatrix} \quad \longrightarrow \quad \sqrt{E}\begin{pmatrix} -\theta/2 \\ 1 \\ \theta/2 \\ -1 \end{pmatrix}$$
$$\Rightarrow \quad \bar{u}_{\text{L}} = \sqrt{E}\left(-\tfrac{\theta}{2}, \quad 1, \quad -\tfrac{\theta}{2}, \quad 1\right) \tag{4.9}$$

$$u_{\text{R}} = \sqrt{E+m}\begin{pmatrix} \cos\frac{\theta}{2} \\ e^{i\phi}\sin\frac{\theta}{2} \\ \frac{|\overrightarrow{p}|}{E+m}e^{i\phi}\cos\frac{\theta}{2} \\ \frac{|\overrightarrow{p}|}{E+m}\sin\frac{\theta}{2} \end{pmatrix} \quad \longrightarrow \quad \sqrt{E}\begin{pmatrix} 1 \\ \theta/2 \\ 1 \\ \theta/2 \end{pmatrix}$$
$$\Rightarrow \quad \bar{u}_{\text{R}} = \sqrt{E}\left(1, \quad \tfrac{\theta}{2}, \quad -1, \quad -\tfrac{\theta}{2}\right) \tag{4.10}$$

where we have indicated the limit of relativistic energies and small emission angles (as discussed in section 4.1.1) by the thin right arrow. The subscripts L and R indicate that the particle is left- or right-handed respectively. The parameters m, $|\overrightarrow{p}|$ and ϕ stand respectively for the particle's mass, three-momentum and azimuthal direction of emission. The former two are cancelled out in the relativistic limit (as then $|\overrightarrow{p}| \approx E \gg m$), while the θ-dependent part is simplified using $\sin\theta \to \theta$ and $\cos\theta \to 1$.

In order to simplify calculations, we assume that the gluons have small virtualities (compared to their squared energies), implying that their polarization directions are perpendicular to their momenta. This lets us decompose any polarization state into two independent components: one that is in the plane of the particle momenta, and one perpendicular to it. Referring back to figure 4.2, we identify the gluon as particle c. The explicit forms of the respective (conjugated) polarization vectors then become (using straight-forward geometry):

$$\begin{aligned} \epsilon^{\text{in}*} &= \left[0, \quad 1, \quad 0, \quad -\theta_c\right] \\ \Rightarrow \quad \epsilon_\mu^{\text{in}*}\gamma^\mu &= -\gamma^1 + \theta_c\gamma^3 \end{aligned} \tag{4.11}$$

[6] The dagger symbol † denotes a Hermitian conjugate, that is, taking the transpose, followed by the complex conjugate.

[7] We do not go through the derivation of these, but they are a well-known result from QFT

$$\begin{aligned} \epsilon^{\text{out}*} &= \begin{bmatrix} 0, & 0, & 1, & 0 \end{bmatrix} \\ \Rightarrow \quad \epsilon_\mu^{\text{out}*}\gamma^\mu &= -\gamma^2 \end{aligned} \tag{4.12}$$

where the superscripts *in* and *out* indicate polarization respectively in and perpendicular to the plane of particle momenta. We have chosen the z-axis to be parallel with the parent particle's momentum, and the x-axis to be in the plane of all the particles' momenta. We have also again used the small-angle approximation.

We now have the explicit forms of every factor in equation (4.8), so that the calculation of the splitting amplitude comes down to straight-forward matrix multiplication. Doing this for the case where both the incoming and outgoing fermion are right-handed, while the gluon is polarized in the plain of particle momenta, yields (using the notation in figure 4.2):

$$V_{qqg}(\mathrm{R},\mathrm{R},\mathrm{in}) = i\, g_s\, T^a_{ij}\, \bar{u}_R(E_b,\theta_b)\, \epsilon^{in*}_\mu\, \gamma^\mu\, u_R(E_a,0) \tag{4.13}$$

$$= g_s\, T^a_{ij}\, \sqrt{E_a E_b}\, (\theta_b + 2\theta_c) \tag{4.14}$$

where E_a and E_b refer to the energies of particles a (incoming fermion) and b (outgoing fermion) respectively.

Equation (4.14) is so far written in terms of E_a, E_b, θ_b and θ_c, but we want to write it instead in terms of t and z (as indicated by equation (4.7), which we are aiming to derive). We therefore take a short detour to find the relationships between these variables. The first of these is of course, by definition, $z = E_b/E_a$.

Next, we use the fact that then momentum of the two particles in the x-direction must cancel. With the small-angle approximation, we have:

$$E_b\theta_b = E_c\theta_c \quad \Rightarrow \quad \frac{\theta_b}{1-z} = \frac{\theta_c}{z}$$

We then define the *total angle* θ,

$$\theta \equiv \theta_b + \theta_c = \theta_b\left(1 + \frac{z}{1-z}\right) = \frac{\theta_b}{1-z},$$

which gives us the next important relationship:

$$\theta = \frac{\theta_b}{1-z} = \frac{\theta_c}{z}. \tag{4.15}$$

Lastly, we demonstrate these variables' relationship to the virtuality $t = k_a^2$, starting with the fact that the four-momentum k_a of the parent particle a must be equal to the sum of the four momenta k_b and k_c of the produced particles:

$$\begin{aligned} t &= (k_b + k_c)^2 \\ &= k_b^2 + k_c^2 + 2k_b \cdot k_c \\ &\simeq 2k_b \cdot k_c \\ &= 2(E_bE_c - \vec{k_b} \cdot \vec{k_c}) \\ &= 2\left(E_bE_c - E_bE_c\left(1 - \frac{\theta^2}{2}\right)\right), \end{aligned}$$

and thus,

$$t = z(1-z)E_a^2\theta^2 \tag{4.16}$$

In the third line we used the relativistic approximation and assumed that that the virtualities of the new particles are much lower than that of the parent particle (see section 4.2), i.e.

$$k_b^2 = t_b \ll t_a, \qquad k_c^2 = t_c \ll t_a.$$

In the fifth line we used the small-angle approximation $\cos\theta \approx 1 - \frac{\theta^2}{2}$.

We are now able to rewrite equation (4.14) in terms of z and t. We first use the definition $z = E_a/E_b$ and equation (4.15) to get

$$V_{qqg}(\mathrm{R},\mathrm{R},\mathrm{in}) = ig_s T_{ij}^a \sqrt{z}[1+z]E_a\theta.$$

We then take the modulus of V_{qgq}, and use equation (4.16) to get

$$\frac{|V_{qqg}|^2}{t^2} = \frac{g_s^2}{t}\cdot\frac{4}{3}\frac{(1+z)^2}{1-z} \tag{4.17}$$

$$\equiv \frac{g_s^2}{t}\cdot F(z). \tag{4.18}$$

As previously indicated, we have summed over i, j and a in the coefficient $|T_{ij}^a|^2$:

$$\sum_{\{a,i,j\}} |T_{ij}^a|^2 = 4 \tag{4.19}$$

Since the index i represents one of three possible colors of the parent quark a, this sum triple-counts three practically identical splittings that we can't distinguish, hence the factor $\frac{1}{3}$ in equation (4.18).

In equation (4.18), we implicitly defined the function $F(z)$ as the z-dependent part of the right-hand side in (4.17). This was however done for the specific case where both quarks are right-handed, and the gluon polarized in the plane of the paper. When calculating $|V_{qqg}|^2$ for any other combination of the particle states (left- or right handed, in- or out-polarized), the result is exactly the same as for equation (4.18), except with a different form of $F(z)$. The form of $F(z)$ for each combination of states is summarized in table 4.1.

In practice we are not interested in the polarizations of the particles that are produced in a cascade. At the same time, we treat left- and right-handed fermions as though they were different types of particles (which table 4.1 confirms that we can do, since the splitting probability is zero if the in- and outgoing quarks don't have matching chiralities). Hence, we take the average of equation (4.18) over the two polarization states, but keeping configurations with different chiralities separate. We hence get:

$$\frac{|V_{qqg}|^2}{t} = \frac{1}{2}\cdot\frac{1}{2}\cdot 4\cdot g_s^2 P(z). \tag{4.20}$$

Table 4.1: Explicit forms of the function $F(z)$ in equation (4.18), corresponding to a given combination of the states of particles a, b and c (see figure 4.2). These forms correspond to the emission of a gluon by a quark ($q \to qg$)

.

a	b	c	$F(z)$
R	R	in	$(4/3)(1+z)^2/(1-z)$
R	R	out	$(4/3)(1-z)^2/(1-z)$
L	L	in	$(4/3)(1+z)^2/(1-z)$
L	L	out	$(4/3)(1-z)^2/(1-z)$
R	L	in	0
R	L	out	0
L	R	in	0
L	R	out	0

Here, the first factor of $\frac{1}{2}$ comes from taking the average of polarization states. The second factor $\frac{1}{2}$, and the following factor 4 is a matter of convention, and we compensate them by including a factor 2 and a factor $\frac{1}{4}$ in the definitino of the *splitting function* $P(z)$ (which we introduced in section 4.1.2):

$$P(z) \equiv 2 \cdot \frac{1}{4} \cdot \sum F(z). \tag{4.21}$$

The summation is over all the combinations of final particle states that may come from a given state of a, and which we do not distinguish. In the present case i.e. where a gluon is emitted by a parent quark, these are all of the configurations (two in total) where the two quarks are left handed. We might as well have chosen the chirality to be right-handed (R), which would have given us the same result. The splitting function for this particular hence has the form

$$P_{qqg}(z) = \frac{4}{3}\frac{1+z^2}{1-z}. \tag{4.22}$$

This splitting function diverges in the limit $1 - z \to 0$, which is as expected, since this corresponds to the emission of very low-energy gluons (see section 4.1.1).

We can now determine the probability that a quark with virtuality t emits a gluon that is characterized by the energy fraction z. By the definition of Feynman amplitudes, this probability can be expressed as

$$\frac{\mathrm{d}\sigma_{n+1}}{\mathrm{d}\sigma_n} = \frac{|A_{n+1}|^2}{|A_n|^2}\frac{\mathrm{d}\Phi_{n+1}}{\mathrm{d}\Phi_n}. \tag{4.23}$$

The factor $|A_{n+1}|^2/|A_n|^2$ is what we have anticipated to find from the discussion in section 4.1.2, and can easily be determined from (4.6). The factors $\mathrm{d}\Phi_n$ and $\mathrm{d}\Phi_{n+1}$ are the respective phase space volumes of the parent particle a and the system of particles $\{b, c\}$ (the second factor on the right thus expresses how many more momentum-states the produced system can have, compared to the parent particle).

Conventionally, their Lorentz-invariant expressions satisfy

$$\mathrm{d}\Phi_n \propto \frac{\mathrm{d}^3 k_a}{(2\pi)^3 2E_a} \tag{4.24}$$

$$\tag{4.25}$$

$$\mathrm{d}\Phi_{n+1} \propto \frac{\mathrm{d}^3 k_b}{(2\pi)^3 2E_b} \frac{\mathrm{d}^3 k_c}{(2\pi)^3 2E_c} \tag{4.26}$$

$$= \frac{\mathrm{d}^3 k_b}{(2\pi)^3 2E_b} \frac{1}{1-z} \frac{\mathrm{d}^3 k_a}{(2\pi)^3 2E_a} \tag{4.27}$$

$$= \mathrm{d}\Phi_n \frac{1}{2(2\pi)^3} \frac{1}{1-z} E_b \, \theta_b \, \mathrm{d}\theta_b \, \mathrm{d}E_b \, \mathrm{d}\phi \tag{4.28}$$

$$= \mathrm{d}\Phi_n \frac{1}{4(2\pi)^3} \mathrm{d}t \, \mathrm{d}z \, \mathrm{d}\phi, \tag{4.29}$$

where ϕ is the azimuthal angle around the direction of the momentum of particle a. We used the fact that

$$\mathrm{d}^3 k_c = \mathrm{d}^3 (k_a - k_b) = \mathrm{d}^3 k_a$$

for constant k_b. Also,

$$\mathrm{d}^3 k_b = |\overrightarrow{k_b}|^2 \sin\theta_b \, \mathrm{d}E_b \, \mathrm{d}\theta_b \, \mathrm{d}\phi \longrightarrow E_b^2 \, \theta_b \, \mathrm{d}E_b \, \mathrm{d}\theta_b \, \mathrm{d}\phi,$$

where we again invoked the relativistic and small-angle limits. Lastly, we made a change of variables from E_b and θ_b to t and z. The easiest way to do this is by the Jacobian method using equations (4.15) and (4.16), as well as $z \equiv E_b/E_a$.

Since there are no variations over the azimuthal angle ϕ, we can integrate it out, getting a factor 2π. Per convention, we absorb the factor 2 into the splitting function, hence the factor 2 in (4.21). With this, equation (4.23) can now easily be rewritten to get exactly equation (4.7):

$$\frac{\mathrm{d}\sigma_{n+1}}{\mathrm{d}\sigma_n} = \frac{\mathrm{d}t}{t} \mathrm{d}z \frac{\alpha_s}{2\pi} P(z),$$

where, again, $\alpha_s \equiv g_s^2/(4\pi)$.

The other two types of splittings that can happen in the QCD cascade are pair production ($g \to qq$) and a triple-gluon splitting ($g \to gg$). The splitting probabilities can be expressed by equation (4.7) as before, only the splitting function $P(z)$ is different. We will go through the derivation of the other splitting functions here, though focusing only on the details that set it apart from the derivation that we just performed. We continue to refer to the particles as a, b and c and use figure 4.2 as reference, with the understanding that different particle types are involved.

For the triple gluon splitting ($g \to gg$), we calculate the splitting function on basis of the triple gluon vertex amplitude, which is [8] [61]

$$V_{ggg} = g_s f^{abc} \left[g_{\sigma\rho} \left(k_a - k_b\right)_\mu + g_{\rho\mu} \left(k_b - k_c\right)_\sigma + g_{\mu\sigma} \left(k_c - k_a\right)_\rho \right] \epsilon_a^\sigma \epsilon_b^{\rho *} \epsilon_c^{\mu *}, \tag{4.30}$$

[8] As always, the Einstein summation convention is implied.

where g_s is the strong coupling constant, $g_{\alpha\beta}$ is the Minkowski metric, and k_i is the four-momentum of particle i (which we define to be positive if pointing inwards to the vertex, and negative if outwards). The factors of the form ϵ_i^α represent the polarization vectors of the particles i. The factor f^{lmn} is a structure constant of the $SU(3)$ algebra (see for example ref. [61]), and the indices $\{l, m, n\}$ are determined by the types of the interacting gluons (they thus span the values $1, 2, ..., 8$). Since the gluon types are inconsequential for our purposes, we will simply sum the (squared) structure constant over these indices, yielding

$$\sum_{\{l,m,n\}} |f^{lmn}|^2 \equiv C_A \tag{4.31}$$

Note that the summation assumes that the incoming gluon state (that is, one of the indices (l, m, n)) is fixed, so as to not triple-count the splitting probability. The factor C_A is called the *color factor*, and it can be shown that it is, for a given N-dimensional Lie group $SU(N)$, equal to N [9] [60], in this case 3.

Using the small angle approximations $\cos\theta \sim 1$ and $\sin\theta \sim \theta$, as well as the relativistic approximation $E^2 = |\vec{p}|^2$, we have

$$\epsilon_a^{in} = \begin{bmatrix} 0, & 1, & 0, & 0 \end{bmatrix} \qquad k_a = \begin{bmatrix} E_a, & 0, & 0, & E_a \end{bmatrix} \tag{4.32}$$

$$\epsilon_b^{in} = \begin{bmatrix} 0, & 1, & 0, & \theta_b \end{bmatrix} \qquad k_b = \begin{bmatrix} E_b, & -E_b\theta_b, & 0, & E_b \end{bmatrix} \tag{4.33}$$

$$\epsilon_c^{in} = \begin{bmatrix} 0, & 1, & 0, & -\theta_c \end{bmatrix} \qquad k_c = \begin{bmatrix} E_b, & E_c\theta_c, & 0, & E_c \end{bmatrix} \tag{4.34}$$

$$\epsilon_a^{out} = \epsilon_b^{out} = \epsilon_c^{out} = \begin{bmatrix} 0, & 0, & 1, & 0 \end{bmatrix}, \tag{4.35}$$

and we use momentum conservation, i.e. $k_a = -k_b - k_c$, to eliminate k_a from the equation.

Calculating explicitly, we again get a vertex amplitude in the form of equation (4.18), though with other forms of the function $F(z)$. We summarize the latter in table 4.2. In this case, we do not distinguish between any of the state configurations, and must therefore take the average over all four of them (we do not consider configurations which don't contribute to the overall probability, i.e. with $F(z) = 0$), introducing a factor $\frac{1}{4}$ in the splitting probability.

Hence, using again definition (4.21), we get the splitting function

$$P_{ggg}(z) = C_A \left[z(1-z) + \frac{z}{1-z} + \frac{1-z}{z} \right]. \tag{4.36}$$

This clearly diverges in the limits $z \to 0$ and $1 - z \to 0$, indicating as expected that the splitting probability becomes large if either gluon is emitted with a low energy.

The third possible splitting channel is pair production, i.e. the production of a quark and an anti-quark[10] by a gluon ($g \to qq$). The fundamental Feynman

[9] As always, the Einstein summation convention is implied.

[10] in general we don't distinguish between particles and their anti-particles in this work, and will (for example) refer to quarks and anti-quarks collectively as quarks.

Table 4.2: Same as table 4.1, except that all of the particles involved are now gluons ($g \to gg$).

a	b	c	$F(z)$
in	in	in	$4C_A\left[z(1-z)+\frac{z}{1-z}+\frac{1-z}{z}\right]$
out	in	in	0
in	out	out	$4C_A z(1-z)$
out	out	out	0
in	in	out	$4C_A\frac{1-z}{z}$
out	in	out	0
in	out	in	0
out	out	in	$4C_A\frac{1}{1-z}$

amplitude is that of a gluon-quark-quark vertex (i.e. $ig_s T^a_{ij}\gamma^\mu$), just as in the first splitting that we looked at (gluon emission by a quark). However, the present splitting involves an outgoing anti-quark in place of an incoming quark. Hence, we need to make use of the (conjugate) Dirac spinors for outgoing *anti-fermions* $\bar{v}^{\rm out}_h$ in place of those for incoming fermions $\bar{u}^{\rm in}_h$. The former are given by

$$v_{\rm L} = \sqrt{E+m}\begin{pmatrix} \frac{|\vec{p}|}{E+m}\sin\frac{\theta}{2} \\ -\frac{|\vec{p}|}{E+m}e^{i\phi}\cos\frac{\theta}{2} \\ -\sin\frac{\theta}{2} \\ e^{i\phi}\cos\frac{\theta}{2}\end{pmatrix} \quad\longrightarrow\quad \sqrt{E}\begin{pmatrix}\theta/2\\-1\\-\theta/2\\1\end{pmatrix} \tag{4.37}$$

$$\Rightarrow\quad \bar{v}_{\rm L} = \sqrt{E}\left(\tfrac{\theta}{2},\quad -1,\quad \tfrac{\theta}{2},\quad -1\right) \tag{4.38}$$

$$v_{\rm R} = \sqrt{E+m}\begin{pmatrix} \frac{|\vec{p}|}{E+m}\cos\frac{\theta}{2} \\ \frac{|\vec{p}|}{E+m}e^{i\phi}\sin\frac{\theta}{2} \\ e^{i\phi}\cos\frac{\theta}{2} \\ \sin\frac{\theta}{2}\end{pmatrix} \quad\longrightarrow\quad \sqrt{E}\begin{pmatrix}1\\\theta/2\\1\\\theta/2\end{pmatrix} \tag{4.39}$$

$$\Rightarrow\quad \bar{v}_{\rm R} = \sqrt{E}\left(1,\quad \tfrac{\theta}{2},\quad -1,\quad -\tfrac{\theta}{2}\right) \tag{4.40}$$

where we have again taken the limit of small emission angles, and relativistic energies. To be clear, $v_{\rm L}$ corresponds to the anti-particle of a left handed quark (and correspondingly for $v_{\rm R}$). The vertex amplitude for pair production is then

$$V_{gqq} \;=\; i\; g_s\; T^a_{ij}\; \bar{u}^{\rm out}_H\; \epsilon_\mu\; \gamma^\mu\; v^{\rm out}_h \tag{4.41}$$

where the notation is the same as in equation (4.8). The polarization vector is no longer complex conjugated, since it corresponds to an incoming gluon, not an outgoing one.

We again assume that the involved gluon is polarized in a direction perpendicular to its direction of motion, and we thus have:

$$\begin{aligned} \epsilon^{\text{in}} &= \begin{bmatrix} 0, & 1, & 0, & 0 \end{bmatrix} & \epsilon^{\text{out}} &= \begin{bmatrix} 0, & 0, & 1, & 0 \end{bmatrix} \\ \Rightarrow \epsilon^{\text{in}}_{\mu}\gamma^{\mu} &= -\gamma^1 & \Rightarrow \epsilon^{\text{out}}_{\mu}\gamma^{\mu} &= -\gamma^2 \end{aligned} \tag{4.42}$$

Doing the matrix multiplications in (4.41) explicitly and expressing the results in terms of z and t as before, we again get the results in the same form as in (4.18). The corresponding functions $F(z)$ for this case are given in table 4.3.

Table 4.3: Same as tables 4.1 and 4.2, except now it concerns pair production ($g \to qq$).

a	b	c	$F(z)$
in	R	R	$(1/2)(1-2z)^2$
out	R	R	$(1/2)$
in	L	L	$(1/2)(1-2z)^2$
out	L	L	$(1/2)$
in	R	L	0
out	R	L	0
in	L	R	0
out	L	R	0

In the same way as we had to include a factor $\frac{1}{3}$ in the splitting probability of gluon emission, we have included a factor $\frac{1}{8}$ for pair production in $F(z)$ here, as the incoming gluon can have eight different colors (which we effectively sum over when we again sum over the indices of T^a_{ij}).

Now, by averaging over polarization states, but keeping chiralities separate, we get the splitting function for pair production:

$$P_{gqq}(z) = \frac{1}{4}[z^2 + (1-z)^2]. \tag{4.43}$$

It is important to note that this is the splitting function for the pair production of either right- or left handed fermions, not both together (which is normally presented in other literature, and has a coefficient $\frac{1}{2}$ instead). We also point out that there are no IR divergences like in the other splitting functions, which implies that pair production does not play a significant role in QCD cascades (or otherwise).

We have thus derived all of the splitting functions involved in this model of a QCD cascade. Equation (4.7) hence tells us the probability that a particle with virtuality t splits into two new particles, where one receives a fraction z of the energy. The same approach can be adapted for cascades involving electroweak interactions, which we will discuss in section 4.3.2. Before that however, we must discuss how the virtuality t evolves with each split.

4.2 Evolution of the Virtuality

As we have indicated earlier, the overarching aim of this chapter is to find expressions for the probability that a particle splits as part of a cascade, which we want to use in a computer simulation to emulate successive splittings and thus a cascade. In the previous sections, we introduced and derived equation (4.7), which we reproduce here for the reader's convenience:

$$\frac{\mathrm{d}\sigma_{n+1}}{\mathrm{d}\sigma_n} = \frac{\mathrm{d}t}{t}\mathrm{d}z\frac{\alpha_s}{2\pi}P(z),$$

This equation implies that for any given splitting, where the parent particle has a given virtuality t, the probability that the energy fraction that is passed on to one of the new particles is equal to z is proportional to $P(z)$. This implies in turn that if it is given that some particle does split, the relative probability that it splits into a particular pair of new particles (that is, into a particular splitting channel) is given by the integral of (4.7) (with the appropriate splitting function $P(z)$) over all the possible values of z. What is not immediately apparent from equation (4.7) is how the virtualities of new particles are distributed. This is because we so far have implied that the variable t, which refers to the virtuality of the parent particle, is determined before the splitting occurs. In truth, we determine it only when the split occurs (which it does not always, since the cascade must stop at some point). Naively then, equation (4.7) says that the splitting probability is completely independent of the parent-particle's state, or the previous history of the cascade. We explain in this section why this is not true[11], and how to realistically model the probability distribution of the parent particle's virtuality. In the process, we will define a condition according to which a particle "choses" to split or not to split.

To begin with, we look at two conditions that are commonly assumed in similar models of particle cascades. First is the assumption that the virtuality is strongly ordered in the cascade [62], meaning that the virtuality of any produced particle is much smaller than that of its parent particle, i.e.

$$t_{\text{old}} \gg t_{\text{new}} \tag{4.44}$$

Technically speaking, we assume that cascades that obey this condition are much more likely than otherwise. This can be most easily be understood by considering that we already assumed $t \ll E^2$ in section 4.1.3 (see the first discussion on gluon polarizations), and the energy E is ordered due to energy conservation. In addition, lower virtualites are in general more likely due to the $\frac{1}{t}$-dependence of equation (4.7).

Secondly, we impose angular ordering of the cascade, meaning that fore each splitting, the angle between two produced particles is always smaller than what it was for the previous splitting, i.e.

$$\theta_{\text{old}} > \theta_{\text{new}} \tag{4.45}$$

[11] We mentioned in section 4.1.2 that the splitting probability was independent of the previous history of the cascade. This was however assuming that the virtuality of the parent particle had already been determined

This condition is actually a consequence of our invocation of the soft limit (see section 4.1.1), and effectively suppresses the otherwise exaggerated emission of low-energy gluons. It is related to the notion that low-energy gluons (i.e. with large de Broglie wavelengths) can only resolve the colour charges of two other gluons if the former is emitted at a smaller angle than the angle between the latter. The exact reasoning and demonstration of these conditions is much more involved, and we refer to the discussions in reference [62]. For the moment, we will only adopt virtuality ordering, to simplify the discussion. We will however adopt angular ordering by the end of the section, as this has been demonstrated to produce more realistic results simulations of parton cascades [62].

Let us consider a particle b that is produced in some splitting, and whose virtuality t we want to know. We know from virtuality ordering that $t < t_a$, where t_a is the virtuality of its parent particle, and acts as a maximum value for t. Despite not knowing the virtuality of b, let us consider the question of whether b will split or not. We *can* find the probability[12] that b *does not* split *nor* has a virtuality t or above. If we denote this probability of *not* splitting as $N(t)$, it must satisfy

$$\frac{\mathrm{d}N}{\mathrm{d}t} = Nf(t), \tag{4.46}$$

where $f(t)$ is the probability of that b splits *given* that it has virtuality t. This is analogous to the nuclear decay problem, in which we would be interested in the probability that an unstable nucleous survives until some time t (although we would then have a minus-sign in equation (4.46), as time is inherently increasing). From section 4.1.1 we know that particle b cannot split if it's virtuality is below some minimal value $t_{\min}$. Thus, $N(t_{\min})$ represents the probability that the particle does not split at all, meaning that it is physical (not virtual) and forms part of the final spectrum of particles that we are trying to determine. The probability $N(t_{\min})$, which also depends on the value of t_a, is often referred to as the **Sudakov form factor**, and denoted by $\Delta(t_a)$.

Keeping with the analogy of nuclear decay, we say that the probability D_{split} that particle b *does* split with some virtuality t is given by $N(t)$, times the probability $f(t)$ that it does split given that it has virtuality t:

$$D_{\text{split}}(t) = N(t)f(t); \qquad f(t) = \frac{1}{t}\sum_i \int_{z_{\min}}^{z_{\max}} \mathrm{d}z \frac{\alpha_i}{2\pi} P_i(z), \tag{4.47}$$

where the index i denotes the splitting channels that are possible for a given parent particle. The expression for $f(t)$ follows directly from equation (4.7), taking into account all the possible z-values that parametrize any given splitting. The argument for equation 4.47 is somewhat more subtle than in the case of nuclear decay, as virtuality is a property of a particle, not a continuously increasing variable like time. It is maybe best understood by going back to the discussion in section 4.1.2. There we explained that the notion that a particle has a certain probability of

[12] Strictly speaking, we mean the *probability density*, as we are talking about probabilities that are functions of the continuous variable t. We drop this technicality in favour of a simpler discussion.

splitting, really means that we consider how the probability for an entire cascade changes if we add one more branch to it (as for example in the transition from figure 4.1a to figure 4.1b). Equation (4.47) hence expresses how the cascade's probability changes if we add a new branch of particles (while assigning a previously unknown virtuality to the parent particle) *without* first adding other branches in-between. In other words, equation (4.7) expresses the probability that a given splitting happens at *any* point in the cascade, while equation (4.47) expresses the probability that the splitting happens *next*. As we simulate the cascade by splitting particles in sequence, we use the latter equation to determine the new virtualities at each point in the cascade.

To find an explicit expression for $N(t)$, we simply integrate equation (4.46) from t_a down to t:

$$N(t) = \exp\left\{-\int_t^{t_a} \mathrm{d}t f(t)\right\} \tag{4.48}$$

What remains is to apply the condition of angular ordering, which will conveniently provide us with suitable cut-off values for the variable z, so that we avoid IR divergences. Motivated by angular ordering, we make a change of variables from z and t, to z and $\tilde{t}$, the latter of which is defined by

$$\tilde{t} \equiv E_a^2 \theta_a^2, \tag{4.49}$$

where E_a is the energy of the parent particle, and θ_a is the angle between the two product particles. With this change of variables, equation (4.7) becomes (using equation (4.16) and the fact that t and z are independent variables)

$$\frac{\mathrm{d}\sigma_{n+1}}{\mathrm{d}\sigma_n} = \frac{\mathrm{d}\tilde{t}}{\tilde{t}}\mathrm{d}z\frac{\alpha_s}{2\pi}P(z), \tag{4.50}$$

Thus, the variable $\tilde{t}$ plays mostly the same role as the variable t has done so far in this discussion. However, the maximum value of $\tilde{t}$ changes significantly. If particle b has energy E_b and its products are separated by an angle θ_b, then angular ordering implies

$$\theta_a^2 > \theta_b^2 \tag{4.51}$$

$$\Rightarrow \quad E_a^2\theta_a^2 > E_a^2\theta_b^2 \tag{4.52}$$

$$\Rightarrow \quad z^2E_a^2\theta_a^2 > E_b\theta_b^2 \tag{4.53}$$

$$\Rightarrow \quad z^2\tilde{t}_a > \tilde{t}_b \tag{4.54}$$

As for the minimum value of $\tilde{t}$, equation (4.16) becomes

$$t \;=\; z(1-z)\tilde{t} \;\leq\; \frac{1}{4}\tilde{t}. \tag{4.55}$$

It is thus natural to set the minimum value of $\tilde{t}$ to

$$\tilde{t}_{\min} = 4t_{\min}, \tag{4.56}$$

so that no value of $\tilde{t}$ will violate the lower bound on the virtuality t. Thus, from equation (4.54), we have that the "choice" of z and t_a for any splitting must satisfy

$$z^2 \tilde{t_a} \overset{!}{>} 4t_{\min},$$

which immediately implies the minimum possible value of z when particle a splits (and by symmetry, the maximum value as well):

$$z \overset{!}{>} \sqrt{\frac{4t_{\min}}{4\tilde{t}}} = \sqrt{\frac{t_{\min}}{\tilde{t}}} \equiv z_{\min} \qquad \Rightarrow \qquad z_{\max} \equiv 1 - \sqrt{\frac{t_{\min}}{\tilde{t}}}. \tag{4.57}$$

The factor 4 in the denominator is necessary to ensure that $z_{\min}$ is always less than 0.5 (as dictated by the conditions $z_{\min} < z_{\max}$ and $z_{\min} + z_{\max} = 1$).

To simplify discussion from here on, we refer to $\tilde{t}$ as the virtuality, and drop the tilde accordingly. Thus, to summarize, every time a particle a splits, its virtuality is subject to the distribution

$$D_{\text{split}}(t) = N(t)f(t); \qquad f(t) = \frac{1}{t}\sum_i \int_{z_{\min}}^{z_{\max}} \mathrm{d}z \frac{\alpha_i}{2\pi} P_i(z), \tag{4.58}$$

as before. However, $N(t)$ is now given by

$$N(t) = \exp\left\{ -\int_t^{t_p z_a^2} \mathrm{d}t f(t) \right\}, \tag{4.59}$$

where t_p denotes the virtuality of a's parent particle, and z_a denotes the fraction of energy that a received from its parent. In the case of the second particle that was produced simultaneously with a, the value of z_a is naturally replaced by $1 - z_a$. The cascade stops if a sample from the distribution (4.58) yields a value that is lower than $4t_{\min}$, where $t_{\min}$ is the minimum virtuality in the original meaning, that is, as it was defined in section 4.1.1.

We point out in the end that angular ordering also implies that the argument of the coupling α (we drop the subscript s, as this pertains to the couplings for both the strong and electroweak interactions) becomes $z^2(1-z)^2 t$ for each splitting, i.e.

$$\alpha = \alpha\left[z^2(1-z)^2 t\right], \tag{4.60}$$

where t is the virtuality in the modified sense (i.e. $\tilde{t}$). We do not go into the reasoning behind this, and refer instead to reference [62].

4.3 Extension to Electroweak Cascading

In section 4 we described a model of parton cascades, i.e. cascades consisting of splittings that happen exclusively via the strong interaction. We now discuss how to take into account electroweak interactions as well, which will allow us to model the cascading of the other particles of the Standard Model (rather than only

quarks and gluons), except the Higgs particle. It turns out that the formalism for electroweak cascades can be expressed in a way that is mostly the same as for QCD cascades, because splitting probabilities can still be expressed in the form of of equation (4.7). The only differences are in effect that the splitting functions $P(z)$ are slightly different (though only up to some constants), and in place of the strong coupling α_s we must naturally use the electroweak coupling α_{ew} (see for example [63]).

We ignore the Higgs for simplification. We expect that the inclusion of the Higgs particle would not play a significant role in the cascade, because it has been shown [8] that IR singularities do not appear in its splitting functions, thus rendering the probabilities of splittings that involve the Higgs particle insignificant compared to others. This is especially the case because the strength of interactions involving Higgs particles are determined by the interacting particles' masses, while we are interested in high-energy scenarios, in which particles effectively behave as though they were massless.

In what follows below, we will discuss the conditions under which we expect electroweak cascades to occur. We will then derive the splitting functions for electroweak splittings, in which we rely heavily on the derivations in sections 4.1.3.

4.3.1 Conditions for Electroweak Cascades

In section 4.1.1 we explained that parton cascades are possible at large energies, because the collinear and soft limits lead to diverging splitting probabilities which compensate the relative smallness of the strong coupling. In the same way, it has been found [8] that when carriers of the electroweak interaction (W bosons, Z bosons, and photons) are emitted at small angles or low energies, this also leads to diverging splitting probabilities. Similarly as in the QCD case, these divergences lead to factors in the splitting interaction probabilities proportional to $\ln^2 \frac{k^2}{m_i^2}$ where k^2 is the squared four-momentum of the parent particle, and m_i denotes the dominating mass of the particles that are produced in a splitting. This sets the lower bound on virtualities at which a particle may split (via the electroweak interaction) to the order of m_i^2, just like in the case of heavy quarks in section 4.1.1.

As we have mentioned previously, in this work we are focusing on cascades initiated by the decay of heavy (dark matter) particles. Denoting the mass of such a particle by m_X, the upper bound on the virtualities of the first two particles in the cascade is given by $(m_X/2)^2$, as the virtuality t is related to energy E and momentum k^2 by

$$t \simeq E^2 - k^2 \leq E^2 = \frac{m_x^2}{4}.$$

The mass-energy of the dark matter particle is divided equally among the initial decay products because we assume the dark matter to be cold, or non-relativistic (see section 3.2), thus having much lower kinetic energy than it has mass. Assuming that the dark matter particle X initially splits into two neutrinos ($X \to \nu\nu$), the

cascading probability can be estimated by finding

$$R = \frac{\Gamma(X \to \nu\nu Z)}{\Gamma(X \to \nu\nu)}, \tag{4.61}$$

that is, the ratio of the probability that the decay produces at least one Z boson to that of it producing merely the two initial neutrinos. This ratio is hence dependent on the logarithm $\ln^2(m_X^2/m_Z^2)$ (where m_Z is the Z boson's mass), and the authors of reference [8] find that R becomes of the order of 0.5 for masses of order 10^6 GeV. We use this criterion to determine the point at which significant cascading occurs, and consider thus dark matter masses of 10^6 GeV and higher throughout this work. For comparison, the Large Hadron Collider has achieved a maximum collision energy of the order 10^4 GeV, making it at present unrealistic to observe electroweak cascading under laboratory conditions.

4.3.2 Splitting Functions for Electroweak Cascades

Having already derived the splitting functions for QCD cascades, it is rather straight-forward to find the splitting functions for electroweak cascades by inspection of the electroweak Feynman amplitudes. This is because each electroweak amplitude is the same as a corresponding amplitude in QCD, up to some constant. Hence it is clear from the derivations of the splitting functions in section 4.1.3, that the electroweak splitting functions will only differ from the ones in QCD by some related constants. This will become clear in the discussion that follows.

We summarize the derivation of the electroweak splitting functions below. The Feynman amplitudes are taken from [61]. We ignore any signs or i-factors, as these would disappear in the rigorous derivation (see section 4.1.3) when the modulus of the splitting amplitude is taken.

We derive first the splitting functions for pair production by Z-bosons ($Z \to ff$), where the produced pari can be any fermion. We use this derivation as a detailed example, allowing us to simplify the remaining derivations thereafter. The vertex amplitude for this splitting is

$$V_{Zff} = \frac{g}{\cos\theta_W}\gamma_\mu \left[\left(\frac{1}{2}\tau_3 - Q\sin^2\theta_W\right)\frac{1-\gamma^5}{2} - Q\left(\sin^2\theta_W\right)\frac{1-\gamma^5}{2}\right]. \tag{4.62}$$

Here, Q is the fermions' charge (relative to the elementary charge); the sign is that of the "ordinary" particle as opposed to the anti-particle. For example, $Q = -1$ for electrons and positrons, and $Q = \frac{2}{3}$ for up and anti-up quarks. The parameter g is the weak coupling constant, analogous to the strong coupling constant g_s. The parameter θ_W is the *Weinberg mixing angle*, and is defined by $\cos\theta_W = m_W/m_Z$, where m_W and m_Z are the masses of the W and Z bosons respectively. The 2 by 2 matrix τ_3 is the Pauli matrix in the z-direction, which is explicitly given by

$$\tau_3 = \begin{pmatrix} 1 & 0 \\ 0 & -1 \end{pmatrix},$$

and acts on a doublet of the form

$$\begin{pmatrix} \nu_l \\ l \end{pmatrix}$$

or

$$\begin{pmatrix} q_u \\ q_d \end{pmatrix}.$$

Here, l is the spinor of a lepton (electron, muon or tau) and ν_l the spinor of its corresponding neutrino. The spinors q_u and q_d represent pairs of up- and down-like quarks (i.e. quarks with $\frac{2}{3}$ or $-\frac{1}{3}$ of an elementary charge). In practice, we may pretend that the matrix τ_3 in equation (4.62) takes a value 1 if the split produces neutrinos or up-like quarks, and -1 otherwise.

Having written the vertex amplitude in the form of (4.62), we can identify the chiral projection operators for left-handed fermions $P_L \equiv (1-\gamma^5)/2$ and for right-handed fermions $P_R \equiv (1+\gamma^5)/2$. This effectively means that the amplitude can be separated into two terms: one proportional to P_L, and one to P_R. The former term is the effective vertex amplitude for a splitting of type $Z \to LL$, i.e. pair production for left-handed fermions:

$$V_{ZLL} = \frac{g}{\cos\theta_W}\gamma_\mu \left(\frac{1}{2}\tau_3 - Q\sin^2\theta_W\right). \tag{4.63}$$

The other term is the effective vertex amplitude for a splitting of type $Z \to RR$ where the fermions are right-handed:

$$V_{ZRR} = \frac{g}{\cos\theta_W}\gamma_\mu Q\sin^2\theta_W. \tag{4.64}$$

In the relativistic limit, left- and right-handed fermions do not mix, and essentially behave like separate kinds of particles. We see that the amplitudes (4.63) and (4.64) have the same form as the amplitude for pair production by gluons ($g \to qq$), which was $ig_s T^a_{ij}\gamma^\mu$, where g_s is the strong coupling constant). To be clear, the expressions have the same form in the sense that they are proportional to γ^μ.

The derivations of the splitting functions for the splittings $Z \to LL$ and $Z \to RR$ now proceed in the exact same way as for $g \to qq$. We short-circuit the derivation for left-handed pair production as follows:

1. We multiply $P_{gqq}(z)$ (equation (4.43)) by 2 in order to compensate for the fact that the generator T^a_{ij} contributed an overall factor of $\frac{4}{8} = \frac{1}{2}$ to $P_{gqq}(z)$.
2. We multiply the result by the square of the scalar coefficient in V_{ZLL} (without the coupling constant g), i.e. $\frac{1}{\cos\theta_W}\left(\frac{1}{2}\tau_3 - Q\sin^2\theta_W\right)$.

Hence, we get

$$P(z)_{ZLL} = \frac{1}{2}\frac{1}{\cos^2\theta_W}\left(\frac{1}{2}\tau_3 - Q\sin^2\theta_W\right)^2\left[z^2 + (1-z)^2\right], \tag{4.65}$$

The derivation of any other pair-producing splitting can be performed in the same way: one multiplies $P_{gqq}(z)$ by 2, and then by the squared scalar coefficient of

the vertex amplitude. The coupling constant g gives rise to the factor α_{ew} in the splitting probability (outside the splitting function) and is therefore left out from this scalar factor. The splitting function for right-handed pair-production hence becomes:

$$P(z)_{ZRR} = \frac{1}{2}\frac{1}{\cos^2\theta_W}\left(Q\sin^2\theta_W\right)^2\left[z^2+(1-z)^2\right]. \tag{4.66}$$

In the same way, we find now the splitting functions for Z boson-emission ($f \to fZ$). Since the vertex amplitude for such a splitting is also given by (4.62), the same arguments apply, only now we look to gluon emission ($q \to qg$) as the analogy from QCD. We find the splitting functions for emission by left-handed fermions as follows:

1. We multiply $P_{qqg}(z)$ (equation (4.22)) by 3/4 in order to compensate for the fact that the generator T^a_{ij} contributed an overall factor of $\frac{4}{3}$ to $P_{qqg}(z)$.
2. We multiply the result by the square of the scalar coefficient in V_{ZLL} (without the coupling constant g), i.e. $\frac{1}{\cos\theta_W}\left(\frac{1}{2}\tau_3 - Q\sin^2\theta_W\right)$.

Thus, we get

$$P(z)_{LLZ} = \frac{1}{\cos^2\theta_W}\left(\frac{1}{2}\tau_3 - Q\sin^2\theta_W\right)^2\left[\frac{1+z^2}{1-z}\right], \tag{4.67}$$

for emission by left-handed fermions, and

$$P(z)_{RRZ} = \frac{1}{\cos^2\theta_W}\left(Q\sin^2\theta_W\right)^2\left[\frac{1+z^2}{1-z}\right]. \tag{4.68}$$

for right-handed fermions.

The same procedure applies to finding the splitting functions for interactions with W-bosons. In contrast to Z bosons, the former must interact with a pair of fermions belonging to the same doublet (see above). In addition, no interactions between W bosons and right-handed fermions are possible. Nevertheless, the familiar form of the vertex amplitudes mean that we can apply the same procedure as above. Starting with pair-production, the vertex amplitudes are

$$V_{Wll} = \frac{g}{\sqrt{2}}\gamma^\mu P_L, \tag{4.69}$$

for leptons, and

$$V_{Wqq} = \frac{g}{\sqrt{2}}C_{ij}\gamma^\mu P_L, \tag{4.70}$$

for quarks. The chiral projector $P_L \equiv (1-\gamma^5)/2$ implies that any multiplication with right-handed spinors will render the amplitudes equal to 0. The factor C_{ij} in (4.70) represents an element of the Cabbibo-Kobayashi-Maskawa (CKM) matrix. The factor arises because the quark mass eigenstates are a superposition of the

quark eigenstates of the weak interaction. The index i refers to the flavour of the up-like quark that is produced in the split, and the element C_{ij} denotes the probability amplitude that the down-like quark will be of flavour j. Apart from these factors, the amplitudes clearly have the same form as before. Hence we find the splitting functions following the same procedure as for the case $Z \to LL$. For lepton production ($W \to \nu l$) we get

$$P(z)_{Wll} = \frac{1}{2} \cdot \frac{1}{2} \left[z^2 + (1-z)^2 \right], \tag{4.71}$$

while for quark production ($W \to q_u q_d$) we get

$$P(z)_{Wqq} = \frac{1}{2} \cdot \frac{1}{2} |C_{ij}|^2 \left[z^2 + (1-z)^2 \right]. \tag{4.72}$$

The splitting functions for W boson emission $f \to fW$ follow straight-forwardly from the procedure that we described for the splitting $L \to LZ$. For emission by leptons ($\nu \to lW$ or $l \to \nu W$) we get

$$P(z)_{llW} = \frac{1}{2} \left[\frac{1+z^2}{1-z} \right], \tag{4.73}$$

and for emission by quarks ($q_u \to q_d W$ or $q_d \to q_u W$) we get

$$P(z)_{qqW} = \frac{1}{2} |C_{ij}|^2 \left[\frac{1+z^2}{1-z} \right]. \tag{4.74}$$

The remaining splitting-types don't distinguish between left- and right handed particles, as they all constitute triple-boson interactions or photon emission (which is chirality-independent). The tripple gluon splittings are W-production by a Z boson ($Z \to WW$), Z-emission by W bosons ($W \to WZ$), and photon emission by W bosons ($W \to W\gamma$) (bremsstrahlung). The vertex amplitudes for these splittings are

$$V_{ZWW} = g \cos\theta_W \left[g_{\sigma\rho} \left(k_{W^+} - k_{W^-} \right)_\mu + g_{\rho\mu} \left(k_{W_-} - k_Z \right)_\sigma + g_{\mu\sigma} \left(k_Z - k_{W_+} \right)_\rho \right], \tag{4.75}$$

for the first two, and

$$V_{WW\gamma} = e \left[g_{\sigma\rho} \left(k_{W^+} - k_{W^-} \right)_\mu + g_{\rho\mu} \left(k_{W_-} - k_Z \right)_\sigma + g_{\mu\sigma} \left(k_Z - k_{W_+} \right)_\rho \right], \tag{4.76}$$

for the latter. Here, $g_{\alpha\beta}$ is the Minkowski metric, and k_i refers to the 4-momentum of particle i (the positive direction is defined towards the vertex). The electric coupling constant e is equal to $g \sin\theta_W$. These vertices clearly have the same form as in the triple-gluon case $g \to gg$ (equation (4.30)) up to the couplings and some constants, and their splitting functions can be derived in the exact same way as $P_{ggg}(z)$ (equation (4.36)). We must only eliminate the factor of 3 that arises from

the coefficient f^{lmn} for the triple gluon vertex, and include the squared coefficient of the vertex amplitudes above. We thus get the splitting functions

$$P_{ZWW}(z) = \cos^2\theta_W \left[z(1-z) + \frac{z}{1-z} + \frac{1-z}{z} \right], \tag{4.77}$$

$$P_{WWZ}(z) = \cos^2\theta_W \left[z(1-z) + \frac{z}{1-z} + \frac{1-z}{z} \right], \tag{4.78}$$

and

$$P_{WWA}(z) = \sin^2\theta_W \left[z(1-z) + \frac{z}{1-z} + \frac{1-z}{z} \right]. \tag{4.79}$$

Now the only remaining splitting that we consider is photon-emission (bremsstrahlung) by charged fermions ($f \to f\gamma$). We do not consider pair production by photons ($\gamma \to ff$) because this does not occur in vacuum. This is because it is impossible to satisfy energy-momentum conservations without additional particle interactions. The vertex amplitude of photon emission has the form

$$V_{ff\gamma} = g(\sin\theta_W) Q \gamma^\mu, \tag{4.80}$$

where Q is the electric charge (in units of the elementary charge) as before. This vertex has, again, the same form as the one for gluon emission ($q \to qg$). Hence, applying the short-circuit derivation from before, the splitting functions become

$$P(z)_{ff\gamma} = \sin^2\theta_W Q^2 \left[\frac{1+z^2}{1-z} \right]. \tag{4.81}$$

We have thus determined all of the splitting functions that we need to describe electroweak interactions between standard model particles.

4.4 Decay and Hadronization

So far, we have discussed how a cascade develops from the initial decay of a dark matter particle, to producing a spectrum of on-shell (that is, physical) particles. However, this spectrum does not correspond to what we expect to observe, because a number of these on-shell particles are themselves unstable, and decay to produce a secondary spectrum. In addition, quarks and gluons don not exist as free particles at low energies (as mentioned in section 4.1.1), but hadronize to produce mesons (mostly pions) and some nucleons. Mesons are also unstable, and decay to produce further neutrinos, photons and electrons. We summarize here how to treat these decays in the context of our model of particle cascades, so that they may be taken into account in our simulations.

4.4.1 Decay of W Bosons, Z Bosons and Top Quarks

The decay of W bosons, Z bosons and top quarks is straight-forward to model, as these are particles with masses that are significantly higher than those of their decay products. This means that we can essentially treat them the same way as we do the initial dark matter particle, splitting them into a pair of initial decay products, and practically starting a new (much smaller) cascade. Quarks other than top quarks do not decay in the same way, despite that some of them have relatively large masses, because they are bound in hadrons on time-scales shorter than their lifetimes.

Since the decaying particles are not generally at rest, we cannot assume that their energies are divided equally among their decay products. However, the distribution of energy fractions attained by either particle is uniform. In other words, if $z = E_b/E_a$, where E_a and E_b are the energies of the decaying particle and one of the product particles respectively, then z follows a uniform distribution. To make this clear, consider a particle at rest that decays into only two particles. In order to conserve momentum, the product particles must have equal and opposite momenta, and thus (in the relativistic limit) equal energies. The only variable in such a decay is the direction into which the product particles are emitted, the probability for which is equal for all angles. Since for any decay, there is a reference frame in which the particle is at rest, and the energy of the particles (in the laboratory frame) can only be dependent on the direction of emission in the rest frame (which is uniformly distributed), the distribution of energies between the two particles must be uniform.

The top quark generally splits into a W boson and a bottom quark, though it has a low probability of producing a down or strange quark instead, due to the non-zero elements of the CKM matrix, as discussed in section 4.3.2. The W and Z bosons have approximately equal probabilities of decaying into each of the possible branching channels that we discussed in section 4.3.2. More precise ratios have however been determined experimentally, and can be found in reference [63].

4.4.2 Decay of Muons and Taus

Muons decay chiefly into a muon-neutrino, electron-neutrino and an electron ($\mu \to \nu_\mu \nu_e e$). Since the decay products consist of three particles (rather than two, as above), the distribution of energies amongst the product particles is not uniform. Analytical calculations yield however that the distribution of energies for the produced neutrinos is given by [64]

$$\frac{\mathrm{d}N_{\nu_e}}{\mathrm{d}z} = 2 - 2z^2 + 4z^3 \qquad \frac{\mathrm{d}N_{\nu_\mu}}{\mathrm{d}z} = \frac{5}{3} - 3z^2 + \frac{4}{3}z^3 \tag{4.82}$$

for electron-neutrinos and muon-neutrinos respectively. The variable z is the fraction of energy that is passed on to the corresponding product particle from the decaying muon. We do not consider the spectrum of electrons produced in these decays, as we are ultimately interested in the final neutrino spectra. Having said this, electron production is not in principle expected to play an insignificant role in

dark matter decays, as it may form a source of cosmic rays and emit secondary radiation in interactions with cosmic magnetic fields and matter. These considerations are however beyond the scope of this work.

In principle, we should also consider the decays of tau leptons in our model. By virtue of their large mass, these particles produce rich decay-spectra, including the production of pions and K-mesons, which decay further to produce neutrinos and photons. However these spectra are not straight-forward to model, and we therefore neglect them in this work. In chapter 6 we argue that the dominant features of a dark matter decay signal of neutrinos is unlikely to be altered by the presence of other particles in the cascades, making this a tolerable concession within the scope of this study.

4.4.3 Hadronization and Decay of Hadrons

We summarize here a phenomenological model of hadronization and subsequent decay that we adopt from [64]. The idea behind it is that when gluons and quarks coalesce, the number of produced hadrons is proportional to the number of quarks and gluons. It is also assumes that the energy spectrum of hadrons that is produced from single partons has the same shape independent of the partons' energies. To make this precise, the spectrum D_h of hadrons (referred to as the fragmentation function) is found from the convolution of the parton spectra D_i with so-called hadronization functions $f_i(z)$:

$$D_h(x, m_X) = \sum_i \int_0^1 \int_0^1 \mathrm{d}x'\mathrm{d}z \; D_i(x', m_X) \; f_i(z) \; \delta(zx' - x) \tag{4.83}$$

$$= \sum_i \int_x^1 \mathrm{d}z \; D_i(x/z, m_X) \; f_i(z) \tag{4.84}$$

As we have indicated, the parton spectra (where the index i goes over the parton types. i.e. gluons and quark flavours) and thus the fragmentation functions are dependent on the mass m_X of the decaying particle, while the hadronization functions are not. The latter makes sense if one assumes that the hadronization process should mostly be dependent on the final states of partons, not on the cascade history. Intuitively then, the model implies that each parton with energy x' (expressed as a fraction of the total cascade energy) produces a spectrum of hadrons of the form $f_i(z)$, where the variable z denotes a fraction of the energy from the parton. We point out again that this is model works on a phenomenological basis, and is not a reflection of the actual hadronization process, which is generally challenging to model.

It is assumed that of the hadrons produced, a fraction $\epsilon_N \approx 0.05$ (based on experimental data) is made up of nucleons, while the rest ϵ_π are mesons [64]. Of the latter, all are taken to be pions. Two thirds of produced pions are expected to be charged, and one third neutral (due to these three particles obeying an approximate isospin symmetry). As we already discussed somewhat in section 2.1, charged pions $\pi^\pm$ decay to form a neutrino and a muon, the latter of which decays

to produce further neutrinos and electrons,

$$\pi^{\pm} \to \nu_\mu \mu; \qquad\qquad \mu \to \nu_\mu \nu_e e,$$

while neutral pions π^0 decay to produce a pair of photons:

$$\pi^0 \to \gamma\gamma. \tag{4.85}$$

We summarize here the formulas by which the expected spectra for neutrinos and photons are found from the fragmentation functions $D_h(x, m_X)$. We are not interested in the spectrum of electrons, as we discussed in section 4.4.2. We do not go into the justifications of these formulae, which we also adopt from reference [64]. The photon spectrum, expressed in terms of the fraction x of the total cascade energy $m_X/2$ is given by

$$\frac{\mathrm{d}N_\gamma}{\mathrm{d}x} = \frac{2}{3}\epsilon_\pi \int_x^1 \frac{\mathrm{d}z}{z} D_h(z, m_X). \tag{4.86}$$

The spectrum of muon-neutrinos, both from charged pion decay and the subsequent muon decay is given by

$$\frac{\mathrm{d}N_{\nu_\mu}}{\mathrm{d}x} = R\int_{Rx}^1 \frac{\mathrm{d}z}{z} D_h(z, m_x) + R\int_x^1 \frac{\mathrm{d}z}{z}\int_z^{z/r} \frac{\mathrm{d}z'}{z'}[\frac{5}{3} - 3z^2 + \frac{4}{3}z^3] D_h(z', m_X). \tag{4.87}$$

The spectrum for electron neutrinos is given by

$$\frac{\mathrm{d}N_{\nu_e}}{\mathrm{d}x} = R\int_x^1 \frac{\mathrm{d}z}{z}\int_z^{z/r} \frac{\mathrm{d}z'}{z'}[2 - 6z^2 + 4z^3] D_h(z', m_X). \tag{4.88}$$

The parameters r and R are related to the ratio of the masses of muons and pions:

$$r = \left(\frac{m_\mu}{m_\pi}\right)^2; \qquad\qquad R = \frac{1}{1-r}.$$

With this, we have almost all the information we need to predict the secondary spectra starting from a parton spectra that is produced in a cascade. What remains is the explicit form of the hadronization functions $f_i(z)$. The authors of [65] suggest hadronization functions of the form

$$f_i(z) = N_i z^{a_i}(z - z_i)^{-b_i}(1 - z)^{c_i}. \tag{4.89}$$

The five constant parameters (which are different for gluons and quarks) are determined by fitting the implied fragmentation functions to empirical pion spectra. Such a fit is dependent on the distribution of partons that is assumed for a given value of m_X, and the hadronization functions may therefore be specific to the particular cascading model that generates the parton spectrum. This means that we can apply the given hadronization functions only if our cascading model is sufficiently similar to that which was used to determine the functions. In addition to

this, it should be mentioned that the parameters of the hadronization functions are fit to emipirical spectra with $m_x = m_Z \approx 91.2\,\mathrm{GeV}$ (the mass of the Z boson), and their independence on m_x does not hold exactly. Their application for values of m_x at orders from $10^6\,\mathrm{GeV}$ to $10^{16}\,\mathrm{GeV}$ may therefore cause significant errors. See reference for a discussion.

We mention briefly here that the provided hadronization functions do not lead to satisfactory results, when applied to our cascading simulations. In particular, the pion spectra that we produce do not match the experimental data to which the hadronization functions originally were fit to. Therefore, it would be necessary to fit new hadronization functions to our particular simulation, if we were to apply this hadronization model. Since this is beyond the scope of this work, we do not consider the hadronization of partons any further in this work.

Chapter 5

Simulating particle cascades

In this chapter, we discuss the methods and algorithms that we use to simulate particle cascades based on the theory in chapter 4. We start by reviewing the mathematical background of the necessary Monte Carlo algorithms, including the veto algorithm. We then describe how these methods are applied to our investigation of particle cascades.

5.1 Principles of Monte Carlo algorithms

Due to the probabilistic nature of quantum field theory (QFT), the simulation of a particle cascade must include some random aspects, or more precisely, sampling from some random variable with a given probability distribution function (PDF). For example, when a particle splits, the virtuality t of the parent particle is not uniquely determined, but chosen randomly from the known PDF given in (4.58). The question is therefore how to simulate the production of samples from such a PDF. If a large number of samples is taken, the distribution of these samples should converge to $D_{\text{split}}(t)$ from equation (4.58) (or whichever PDF we are interested in simulating). In answering this question, we follow closely the work of [66]. We will assume that we have a means of producing samples from a uniform random variable R with a range of 0 to 1. We will refer to the random variable that we want to sample by X and to its PDF as $f_X(x)$. We point out that the random variables that we are interested in sampling in our investigation are the virtualities t and the energy fractions z of particles (see section 4.1.2); nevertheless we refer to the more general variable x in this section, in order to emphasize the generality of the mathematics that we present.

We can easily relate the general random variable X to the uniform random variable R by

$$\int_{x_{\min}}^{X} f_X(x)\mathrm{d}x = R,$$

where we have assumed that $f_X(x)$ is normalized to 1. In other words, $\int_{x_{\min}}^{x} f_X(x)\mathrm{d}x = r$, where x and r are samples of the random variables X and R respectively. The

minimal possible sample of X is given by $x_{\min}$. This expression is equivalent to the intuitive statement that the cumulative probability of a sample of X (or any random variable) is uniformly distributed. If $f_X(x)$ is not normalized to 1 (i.e. it is not strictly speaking a PDF, but proportional to one), we only have to multiply the right-hand side with the normalization constant, that is

$$\int_{x_{\min}}^{X} f_X(x)\mathrm{d}x = R \int_{x_{\min}}^{x_{\max}} f_X(x)\mathrm{d}x. \tag{5.1}$$

If we define $F(x)$ so that $\frac{\mathrm{d}F}{\mathrm{d}x} = f_X(x)$ (i.e. $F(x)$ is the cumulative distribution of $f_X(x)$), then we get

$$X = F^{-1}\left(F(x_{\min}) + R[\,F(x_{\max}) - F(x_{\min})\,]\right).$$

This would make the production of samples from X straight-forward, given a sample from R. However it is required that we can find an anti-derivative of $f_X(x)$ that also has a well-defined inverse, which is not the case for the distributions that we will look at when simulating particle cascades (see Section 5.2).

There is a simple work-around to this problem. Instead of producing a sample from the distribution $f_X(x)$, we find a distribution $g(x)$ for which we can find an anti-derivative, and for which $g(x) \geq f_X(x)\ \forall\ x$. The algorithm for producing a sample from $f_X(x)$ is then as follows (we refer to this as **algorithm A** for future reference):

1. produce a sample from $g(x)$ as described above, that is, set

   $$x = G^{-1}\left(G(x_{\min}) + r_1[\,G(x_{\max}) - G(x_{\min})\,]\right)$$

   for $\frac{\mathrm{d}G}{\mathrm{d}x} = g(x)$, where r_1 is a sample from a uniform distribution.

2. Produce another sample r_2 from R. If $r_2 > f_X(x)/g(x)$, then ignore this value of x and start again at step number 1. If on the other hand $r_2 < f_X(x)/g(x)$, use this value of x as the sample from $f_X(x)$.

The sample x that is produced from $g(x)$ has, by the way that we defined it, a probability $g(x)\mathrm{d}x$ of being chosen in step 1. In step 2, by the nature of the uniform distribution, there is a probability $f_X(x)/g(x)$ of the value being kept, rather than rejected. Hence the probability of x resulting from the algorithm is $(f_X(x)/g(x))g(x)\mathrm{d}x = f_X(x)\mathrm{d}x$, which is the defining property of a sample $f_X(x)$.

It is worth mentioning that some choices for the function $g(x)$, though technically viable, are not practical because they are "too different" from $f_X(x)$. More concretely, $g(x)$ may be much greater than $f_X(x)$ for significant ranges of x, meaning that there is a large probability that the value of x chosen in step 1 will ultimately be rejected in step 2. In this case, the simulation could effectively run for an unreasonable amount of time.

The algorithm above is useful for drawing samples from some probability distributions, including for the energy fraction z of a particle that is produced bye some splitting in a cascade. However, for producing samples from $D_{\text{split}}(t)$ in (4.58), we

prefer another, more expedient scheme. This is because $D_{\text{split}}(t)$ contains an exponential over a double integral, multiplied by yet another integral. We use instead the so-called **veto algorithm** [66], for which it suffices to work only with the function $f(t)$ (not to be confused with the PDF $f_X(x)$). The function $f(t)$ is defined by equation (4.58), and completely determines $D_{\text{split}}(t)$ (given some maximum value of t). Hence, the veto algorithm does not only make our work significantly less cumbersome, but also decreases our dependency on robust numerical integration methods as well as computing power. We summarize the algorithm first, and explain why it works thereafter. We continue to use x to denote our sample (rather than t), in order to maintain continuity.

The veto algorithm assumes that the PDF from which a sample x is to be drawn has the form

$$f_X(x) = h(x) \exp\left\{ -\int_x^{x_{\max}} h(x')\mathrm{d}x' \right\},$$

where $x_{\max}$ is the maximal x-value that can be chosen. Notice that this is exactly the expression for D_{split}, if we make the substitutions $x \to t$, $f_X(x) \to D_{\text{split}}$ and $h(x) \to f(t)$. A function $g(x)$ has to be chosen so that $g(x) \geq h(x)\ \forall\ x$, and so that an anti-derivative $G(x)$ with a valid inverse $G^{-1}(x)$ can be found. The algorithm is then as follows:

1. Set $i = 0$ and $x_0 = x_{\max}$
2. Chose a random number $R = r_1$ from the uniform random distribution. Add 1 to i, and set $x_i = G^{-1}\left(G(x_{i-1} + \ln r_1)\right)$.
3. If $x_i \geq x_{i-1}$ disregard this value, and chose a new one via step 2.
4. Chose a new sample from the uniform distribution, $R = r_2$. If $r_2 \geq h(x_i)/g(x_i)$, then ignore x_i and return to point 2. Otherwise, x_i is the final sample from $f_X(x)$.

This algorithm does not easily make intuitive sense, but it is not very complicated to show that it works mathematically. Starting at step 2, a value x_i is chosen so that it can be regarded as sample from a distribution with the form

$$f_g(x_i) = g(x_i) \exp\left\{ -\int_{x_i}^{x_{\max}} g(x_i')\mathrm{d}x_i' \right\}.$$

To see this, consider that for the same reason that (5.1) is true, we have that

$$1 - R = \int_{X_i}^{x_{\max}} f_g(x_i')\mathrm{d}x_i' = 1 - \exp\left\{ -\int_{X_i}^{x_{\max}} g(x_i')\mathrm{d}x_i' \right\},$$

where we for simplicity have assumed that $g(x_{\max}) = 1$, and that $f_g(x)$ is normalized to 1 (but the final result does not depend on these assumptions, as can easily be checked). We have replaced R with $1 - R$ for convenience, though these effectively are the same random variable. Solving, it follows directly that X_i is given by

$$X_i = G^{-1}(G(x_{i-1} + \ln R)).$$

The proof that the algorithm works now follows from writing down the the probability (technically the probability density) that a sample of $f_g(x)$ has a certain value, given that it is found on the i^{th} try, in other words, after $i-1$ samples have already been rejected by step 4. We denote this probability by $f_i(x)$. For example, the probability that the sample x is produced, given that no intermediate samples have to be rejected is

$$f_1(x) = g(x) \exp\left\{ - \int_x^{x_{\max}} g(x') \mathrm{d}x' \right\} \frac{h(x)}{g(x)}, \tag{5.2}$$

where the fraction follows from step 4, and the rest from step 2. The explicit form of $f_2(x)$ becomes:

$$f_2(x) = \int_x^{x_{\max}} g(x_1) \exp\left\{ - \int_{x_1}^{x_{\max}} g(x') \mathrm{d}x' \right\} \left(1 - \frac{h(x_1)}{g(x_1)} \right) \mathrm{d}x_1 \cdot g(x) \exp\left\{ - \int_x^{x_1} g(x') \mathrm{d}x' \right\} \frac{h(x)}{g(x)}, \tag{5.3}$$

where the factor $\left(1 - \frac{h(x_1)}{g(x_1)}\right)$ arises because the first intermediate sample x_1 must be rejected by step 4, and everything to the left of it represents the probability that the value x_1 is chosen by step 2 in the first place. The integral is necessary because all possible values of x_1, which must be less thant x, must be considered. The remaining factors are the probability that x is chosen at the second try, and is analogous to (5.2); however notice that the integration starts at x_1 by virtue of step 3. Simplification yields

$$f_2(x) = f_1(x) \int_x^{x_{\max}} [g(x_1) - h(x_1)] \, \mathrm{d}x_1. \tag{5.4}$$

Following directly analogous steps, $f_3(x)$ becomes

$$f_2(x) = f_1(x) \int_x^{x_{\max}} [g(x_1) - h(x_1)] \, \mathrm{d}x_1 \int_x^{x_1} [g(x_2) - f(x_2)] \, \mathrm{d}x_2 \tag{5.5}$$

$$= \frac{1}{2} f_1(x) \left(\int_x^{x_{\max}} [g(x') - h(x')] \, \mathrm{d}x' \right)^2. \tag{5.6}$$

The second step derives from the general result

$$\int_x^{x_{\max}} \mathrm{d}x' u(x') \int_x^{x'} \mathrm{d}x'' u(x'') = \frac{1}{2} \int_x^{x_{\max}} \mathrm{d}x' u(x') \int_x^{x'} \mathrm{d}x'' u(x'') + \frac{1}{2} \int_x^{x_{\max}} \mathrm{d}x'' u(x'') \int_x^{x''} \mathrm{d}x' u(x') \tag{5.7}$$

$$= \frac{1}{2} \left(\int_x^{x_{\max}} \mathrm{d}x' u(x') \right)^2. \tag{5.8}$$

We can generalize $f_i(x)$ to

$$f_i(x) = \frac{1}{i!} f_1(x) \left(\int_x^{x_{\max}} [g(x') - h(x')] \, \mathrm{d}x' \right)^i . \tag{5.9}$$

Hence, since by definition

$$f_X(x) = \sum_{i=0}^{\infty} f_i(x),$$

we get

$$f_X(x) = f_1(x) \sum_{i=0}^{\infty} \frac{1}{i!} f_1(x) \left(\int_x^{x_{\max}} [g(x') - h(x')] \, \mathrm{d}x' \right)^i \tag{5.10}$$

$$= g(x) \exp\left\{ - \int_x^{x_{\max}} g(x') \mathrm{d}x' \right\} \frac{h(x)}{g(x)} \exp\left(\int_x^{x_{\max}} [g(x') - h(x')] \, \mathrm{d}x' \right) \tag{5.11}$$

$$= h(x) \exp\left(- \int_x^{x_{\max}} h(x') \mathrm{d}x' \right), \tag{5.12}$$

which is the defining requirement for x to be a sample of $f_X(x)$.

5.2 Application of MC Algorithms

In this section, we describe the defining features of our particle cascade simulation, i.e. we will summarize the details that should be sufficient to reproduce our results (which we present in chapter 6). In short, the simulation takes as input a defining set of parameters, which represent properties of a (dark matter) particle that decays, and hence initiates a cascade. Specifically, these parameters are the particle's mass, as well as a specification of which particles it decays into. As output, the simulation yields a list of data sets, which represent the final particles that are produced by the cascade and their properties. These properties are specifically the particle types and the values of their energies.

To keep track of the particles involved in the simulated cascade, our program maintains a stack of virtual particles, represented by data sets. These particles have been produced by preceding splits, but have not yet split themselves. The data sets contain values of important particle parameters: their types, energies, maximum virtualities, and chiralities (whether they are left- or right-handed). The first data set that is put in the stack during the simulation represents the particle which the dark matter particle is defined to decay into, for example a neutrino. It is generally assumed that at least two new particles would be produced in a dark matter decay, but since both set off statistically equivalent cascades, this doesn't affect the final spectra. The energy that is ascribed to this first particle is half of the decaying particle's mass, i.e. $m_X/2$, as we assume that the dark matter is immobile (compared to the speed of light, see section 3.2). The two first particles, and thus the two produced jets, must therefore share their total energy equally. By

the same virtue, the new particles' maximum virtualities are set to $(m_X)^2$, as the virtuality $t = k^2 = E^2 - p^2$ cannot be larger than the squared energy, E^2.

To simulate a cascade, our program repeatedly removes the top particle in the stack, and decides whether this particle should split or not; if it does, two new particle datasets, corresponding to the produced particles, are placed on top of the stack. If the particle does not split, it's energy and type are stored, and no new particles are added to the stack. Whether or not a particle splits is determined by producing a sample from the virtuality-dependent distribution given by equation (4.58), which we write explicitly here for the reader's convenience:

$$D_{\text{split}}(t) = N(t)f(t); \qquad f(t) = \frac{1}{t}\sum_i \int_{z_{\min}}^{z_{\max}} \mathrm{d}z \frac{\alpha_i}{2\pi} P_i(z),$$

with

$$N(t) = \exp\left\{ -\int_t^{t_{\mathrm{p}} z^2} \mathrm{d}t f(t) \right\}.$$

As introduced in section 4.2, the index i refers to the possible splitting channels of the particle, and $t_{\max}$ denotes the particle's maximum virtuality. To produce a sample from this distribution, we use the veto algorithm as described in section 5.1. The integral over z is evaluated numerically. We choose the function $g(t)$ to be proportional to $1/t$. This makes it straight-forward to find the antiderivative $G(t) \backsim \ln(t)$ and its inverse $G^{-1}(x) \backsim \exp\{x\}$. In addition, this choice of $g(t)$ has a similar shape to $f(t)$ in (5.15), making simulations reasonably quick. In order to fulfill the requirement that $g(t) \geq f(t)\ \forall\ t$, experience shows that it suffices to normalize $g(t)$ so that $g(t_{\max}) = 8f(t_{\max})$, which still maintains reasonable simulation speeds.

As we discussed in section 4.2, if the chosen sample t is lower than the minimal virtuality $t_{\min}$, then the particle does not split (hence is real and has virtuality 0), and it's parameters are stored for later analysis. Conversely, if $t > t_{\min}$, then the particle *does* split, and t is it's virtuality. The maximum possible virtualities of the produced particles are set to tz^2 and $t(1-z)^2$, where z and $(1-z)$ are the new particles' respective energies as fractions of the parent particle's energy. How the value of z is determined is discussed below.

However, before z is sampled for a given splitting, the splitting channel is decided on. This can be done assuming that the value of t of the splitting parent particle has already been determined. Choosing the splitting channel is then achieved in rather straight-forward, by computing the value of $f(t)$ for each channel by numerical integration. The ratios of the values of $f(t)$ are equal to the ratios of the channel probabilities (see section 4.2). Thus, a channel can be chosen by dividing up the interval $[0, 1]$ according to the relative values of $f(t)$ and seeing in which of the intervals a sample of a uniform random variable generator falls. As indicated in section 4.3.2, left- and right-handed particles are treated as separate types of particles, so that splittings that involve particles with different chiralities are also treated as separate splitting channels.

After the virtuality t and the splitting channel i, the energy fraction z (and $1 - z$) attained by the produced particles is the third and last random aspect of

any given splitting in the simulation. Having determined the splitting channel, the z-distribution is given by the corresponding splitting function $P_i(z)$ times the corresponding coupling constant $\alpha(z^2(1-z)^2t)$ (for strong or electroweak interactions), though bounded from above and below by $z_{\min}$ and $z_{\max}$. Samples from this distribution can be generated using algorithm A from section 5.1. Here, the combined function $\alpha(z^2(1-z)^2t)P_i(z)$ takes the place of the distribution function $f_X(x)$. The function $g(x)$ (or $g(z)$, using the correct variable) is required to satisfy $g(z) \geq \alpha(z^2(1-z)^2t)P(z)\forall z$, and has to have an invertible antiderivative. In order to make $g(z)$ similar to $P_i(z)$, we use a different function depending on the channel type, that is, depending on what combination of bosons and fermions is interacting (since splits of the same type have the same splitting functions, up to some constant). We summarize the chosen functions $g(z)$ and their anti-derivatives for each case here:

boson → boson boson

$$\frac{\alpha_i}{2\pi}P_i(z) = \Lambda\frac{\alpha_i}{2\pi}\left[\frac{z}{1-z} + \frac{1-z}{z} + z(1-z)\right]; \quad g(z) = \Lambda\frac{\alpha_i^*}{2\pi}\left[\frac{1}{1-z} + \frac{1}{z}\right] \tag{5.13}$$

boson → fermion fermion

$$\frac{\alpha_i}{2\pi}P_i(z) = \Lambda\frac{\alpha_i}{2\pi}\left[z^2 + (1-z)^2\right]; \qquad g(z) = \Lambda\frac{\alpha_i^*}{2\pi} \tag{5.14}$$

fermion → fermion boson

$$\frac{\alpha_i}{2\pi}P_i(z) = \Lambda\frac{\alpha_i}{2\pi}\left[\frac{1+z^2}{1-z}\right]; \qquad g(z) = \Lambda\frac{\alpha_i^*}{2\pi}\left[\frac{2}{1-z}\right] \tag{5.15}$$

For notational clarity, α_i is implicitly a function of z, and we have introduced $\alpha_i^* \equiv \alpha_i(z_{\min}^2(1-z_{\min})^2t)$. Since $z_{\min}^2(1-z_{\min})^2t \leq z^2(1-z)^2t$, and the coupling constants increase with decreasing arguments, this ensures that $g(z)$ is larger than the distribution function, no matter the value of the coupling. By Λ we mean any constant that occurs in the splitting function, for example $\cos^2\theta_W$ for the case $Z \to WW$ (see equation (4.77) and section 4.3.2). In practice, we don't need to worry about this constant, nor the factor $1/2\pi$, since these are cancelled by the algorithm in taking the fraction $f(z)/g(z)$.

After z has been set, the two new particles' absolute energies are determined by multiplying the splitting particle's energy by z and $1-z$ respectively. Thus the entire datasets corresponding to the new particles have been determined and are placed on top of the stack.

Hence, the entire process is repeated with the particle that is now on the top of the stack. Every time a particle does not split, and the particle is stable, it's type and energy is stored in the final output. If the particle is unstable however, the simulation produces a new set of particles corresponding to its decay products.

When a particle is found not to split, our program starts a decay routine that is specialized for each particle. In most cases, the particle's energy and type are simply stored for later analysis. However, in the cases where the particle is unstable (see section 4.4), new particles are placed in the stack according to what is expected of the decay products. In the cases of W bosons, Z bosons and top quarks, a decay channel is chosen based on the empirical fragmentation ratios. The energy passed to each particle is then determined by choosing a z-value from a uniform distribution. The maximum virtuality is set to be the square of the particle's energy. For muon decay, we apply Algorithm A to determine the z-values of the neutrinos from the distribution functions (4.82). We use $g(z) = 2\cos\left(\frac{\pi}{4}z\right)$.

Since the involved virtualities decrease consistently with every splitting, at some point no more particles will split, and the stack will become empty. At this point, the cascade is finished. The final output is thus a list of particles along with their types and energies, which are ready for analysis.

Chapter 6

First Results

In this work, we have focused on the theoretical and practical framework of how particle cascades can be simulated that take into account both the strong and electroweak interactions, thus allowing for most of the standard model particles to be included. Before we summarize, we turn briefly to look at the results of the simulating program that we have thus devised. We make some assessments as to the soundness of the results, and analyse some of the main features of particle cascades. We will thus be able to discuss the outlook of this research, and we discuss its application to the search for superheavy dark matter.

We start with an analysis of the properties of parton cascades, before we look at cascades that involve electroweak interactions and the full range of SM particles. One important reason for this is that parton cascades have been simulated in other works according to schemes that are essentially the same as the ones that we employ. This allows us to compare our results for parton cascades to results from the literature, which we expect to be very similar. We thus aim to confirm that the computer program that we use indeed reflects the physical model that we have described, and is not prone to serious error. Such an affirmation should largely carry over to simulations of the electroweak sector as our program is identical for both sectors, except for the input of concrete physical variables such as particle types, couplings, coefficients in the splitting functions and cut-offs.

Another reason to look at parton cascades is that the probability for a quark to emit a gluon is, for all relevant virtualities, much higher than that of emitting a W or Z boson, as we will see. This means that once any cascade produces as quark, that quark will essentially start a separate parton cascade, as there is no probable way in which that quark or its products can give rise to particles that are not partons. Hence, a cascade that starts with an electroweak interaction can for all practical purposes be separated into an electroweak part and a strongly interacting one. It is thus convenient to analyse QCD cascades and electroweak ones separately.

We will analyse electroweak cascades in a similar fashion. In addition to corroborating our results with other simulations (to the degree that these are available), we discuss what degree of significance different aspects of the simulations (elec-

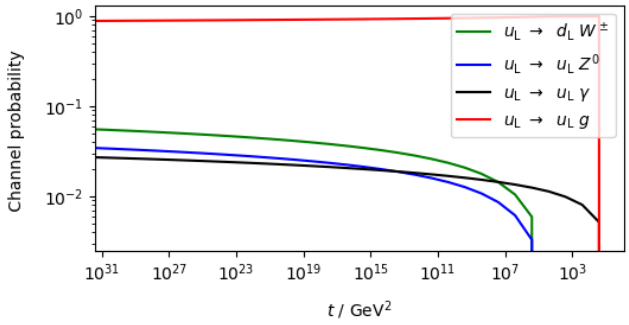

Figure 6.1: Probabilities of an up-quark to decay into the indicated channels. These analytic distributions are proportional to the values of $f(t)$ given by equation (4.58), as discussed in section 5.2. The d in the channel for W-emission includes all down-like quarks. Each channel has a probability of zero below its respective minimal virtuality (see section 4.2). While this figure concerns a left-handed up-quark, the situation is similar for right-handed quarks.

troweak sector, QCD sector, hadronic decays, decays of other particles) carry in terms of the final neutrino spectra. This is crucial in order to identify potential weaknesses in our model and method, and to point out future amendments or research prospects.

6.1 QCD sector

We start by confirming the claim that quarks have a low probability of emitting a W-boson or Z-boson, compared to that of emitting a gluon. Figures INSERT illustrate the probability for an up-quark to decay into each of it's possible channels, at a given virtuality. The channel probablilities for the other five quarks develop in a similar fashion. It is clear that the probability of the channels where a W- or Z-boson is emitted to occur are negligible over the whole range of virtualities. Gluon emission thus remains the dominant channel of splitting for quarks down to virtualities to the scale of the QCD cut-off $10 \times \Lambda^2_{QCD}$. Given the similarity of these processes' splitting functions, this is a demonstration of the difference in scale between the strong couplings and the electroweak coupling.

As a test of our program's validity, we compare the results of pure gluon cascades (i.e. cascades involving gluons only) from our simulations to those from reference [62]. The resulting spectra are shown in figure 6.2. The simulation from the literature largely follows the same principles as our own in the QCD cascading sector. We indeed see that the spectra come out with the same normalization, though with some minor differences in width and position of the peak. Small differences are to be expected as we use a different value of the the QCD cut-off Λ^2_{QCD} as well as a more precise approximation of the strong coupling.

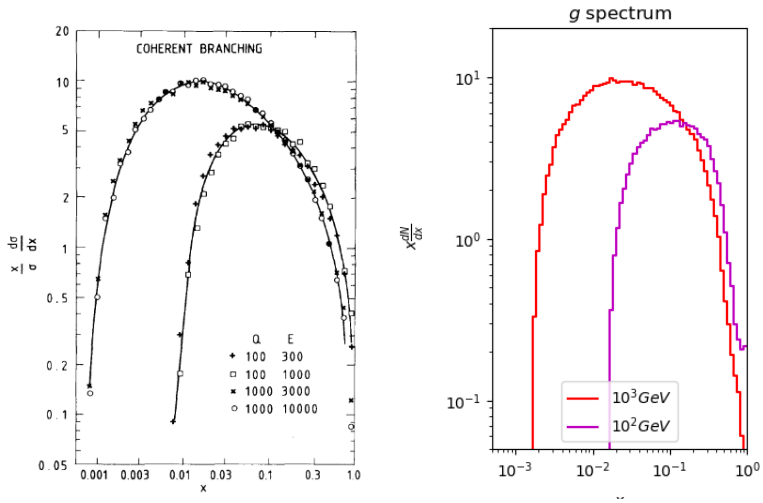

(a) (b)

Figure 6.2: Comparison of the spectra of a pure gluon cascade, starting with a particle of the indicated mass (denoted by Q in a). The spectrum in a was produced from simulations by the authors of ref. [62], while the one in b was produced by our simulation. The independent variable x denotes energy expressed as a fraction of the total cascade energy.

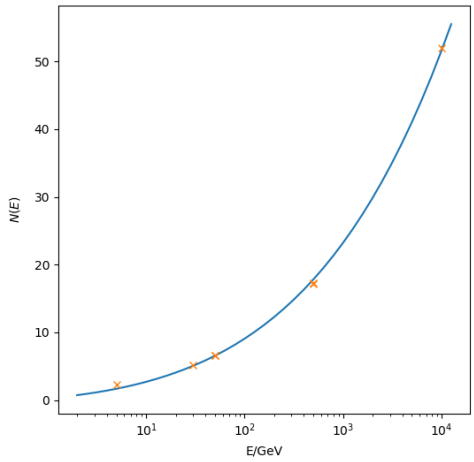

Figure 6.3: Variation of the multiplicity of a pure gluon cascade with the energy of the first particle. Crosses represent simulated values, while the curve is given by equation (6.1).

As another way to probe the consistency of the gluon sector of our simulation, we compare the average multiplicities (numbers) $N(E_{jet})$ of gluons produced in a cascade to the analytical expectation [62]:

$$N(E_{jet} \propto \left(\ln \frac{E_{jet}}{\sqrt{10} \times \Lambda_{QCD}} \right)^{-\frac{1}{4}} \exp \left[\left(\frac{48}{11} \ln \frac{E_{jet}}{\Lambda_{QCD}} \right)^{\frac{1}{2}} \right] \tag{6.1}$$

To clarify, E_{jet} represents the energy of the first particle in the simulation, not the implied on-shell (dark matter) particle, which has twice that energy. We have also replaced the cut-off used in ref. [62] by the cut-off that we use in our simulation, namely $t_{min} = 10 \times \Lambda_{QCD}^2$. Using these facts, we see that the simulated results indeed match the analytical expectation very well, given a suitable proportionality constant (figure 6.3).

The comparisons we have made above assume cascades that are made up of gluons only, and no quarks. Results for the spectrum of a complete parton cascade using the same Monte Carlo scheme as we do are not as readily available in the literature as for only gluons. However, it is expected that the total multiplicity (gluons and quarks) of a cascade that is started by a gluon is higher than if it were started by a quark, and furthermore, that the ratio between these average multiplicities is $9/4 = 2.25$ in the limit of very large total energies. In addition, the authors of reference [67] found for a Monte Carlo scheme similar to ours, that the convergence is linear in the variable $(\ln(E_{jet}/\Lambda)^{0.5}$, where Λ represents the cut-off scale, which we replace it by $\sqrt{10} \times \Lambda_{QCD}$. Plotting the ratios obtained by our simulation against this variable (figure 6.4) reveal that they do plausibly

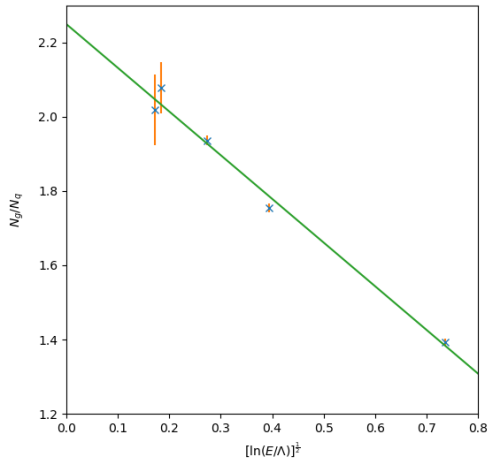

Figure 6.4

Figure 6.5: Variation with the total cascade energy of the ratio $\frac{N_g}{N_q}$, where N_g and N_q are the average multiplicities of cascades that start with a gluon or a quark respectively. Crosses indicate results from our simulation, and the error bars are given by the standard error of the multiplicities between individual cascades. The best-fit line with an intercept equal to 9/4 is indicated.

converge towards the value 9/4 in a linear fashion. It therefore seems as though our simulations match expectations rather well. By the nature of our simulating scheme, the QCD and electroweak sectors of cascades differ only by a concrete set of parameters, not in any methodology. Hence, we take the good results from the QCD sector as an indicator that our simulation as a whole is not prone to significant technical errors.

6.2 Electroweak Sector

We now turn to review the results of cascades in which electroweak interactions play a more significant role. We demonstrated in section 6.1 that any quark that appears in a cascade will for all practical purposes produce a subcascade of only gluons and more quarks if it splits. However, the other particles of the standard model can play a larger role if the particle that starts the cascade is neither quark nor gluon, meaning that it does not interact via the strong coupling. In such a scenario, the carriers of the weak interaction – W and Z bosons – play a similar role to that which the gluon plays in a parton cascade. In fact, if the first particle of the cascade is a neutrino (a scenario that we singled out in particular in section 2.1), the only possible splittings that could happen next are the emission of either

Table 6.1: Approximate proportions of the total cascading energy m_X residing in each type of particle in the final state, for different values of m_X. The starting particle is a neutrino. It is that all particles are stable, that is, they don't decay after they become on-shell.

m_X/GeV	W	Z	γ	ν	l	$q+g$
10^6	0.04	0.02	0.01	0.7	0.2	0.003
10^{11}	0.09	0.04	0.05	0.4	0.4	0.007
10^{16}	0.1	0.04	0.07	0.3	0.4	0.02

boson, i.e.

$$\nu \;\rightarrow\; e\,W \qquad\qquad \text{or} \qquad\qquad \nu \;\rightarrow\; \nu\,Z,$$

which happen with similar probabilities, by virtue of their similar splitting functions (see equations (4.67) and (4.73)). The emitted bosons can in principle produce any type of fermion via pair-production splits, but this is relatively unlikely due to the lack of divergences in the splitting functions of these splitting channels (see section 4.3). Typically, the bosons will split to produce more W and Z bosons, as well as photons:

$$W \;\rightarrow\; W\,Z, \qquad\qquad W \;\rightarrow\; W\,\gamma, \qquad\qquad Z \;\rightarrow\; W\,W.$$

It is thus reasonable to picture the electroweak cascades as dominated by splittings of W and Z bosons, which split to produce more of themselves, in addition to photons. We can make a first assessment of this picture by looking at table 6.1, which summarizes the approximate proportions of the total cascade energy that would be carried by each type particle if we ignored the decay of unstable particles. It is striking that the total share of energy actually seems dominated by neutrinos and leptons. The reason for this is that the cascades that we have simulated have electron-neutrinos as the staring particle. If we look at the energy-proportions of muon- and tau-neutrinos separately, we find that these are on the order of gluons and quarks. The large neutrino component thus comes from the fact that many of the starting neutrinos do not split often enough to lose most of their energy. Similarly, the large lepton component is dominated by the energy in electrons, indicating that many energetic electrons are produced from W-emissions by the starting neutrinos. Other than this, the dominant component of energy is made up by W and Z bosons and photons for all cascading energies. We include for completeness the proportions after the decay of unstable particles (table 6.2), and see that while this causes significant increases to energy of partons, but the abosolute amounts are insignificant compared to the total neutrino and lepton energy. It is thus clear, that the most natural way in which dark matter may produce detectable neutrino signals is by coupling directly to them, as other channels would produce less intense fluxes. The resulting spectrum (figure 6.6) is strictly increasing towards higher energies, and most notably features a sharp peak towards the value of the dark matter mass. A natural signal of dark matter decay to look for is thus some

Table 6.2: Approximate proportions of the total cascading energy m_X residing in each type of particle in the final state, for different values of m_X. The starting particle is a neutrino. These values take into account the decay of unstable particles.

m_X/GeV	γ	ν	l	$q+g$
10^6	0.01	0.7	0.2	0.03
10^{11}	0.05	0.4	0.4	0.08
10^{16}	0.09	0.3	0.5	0.1

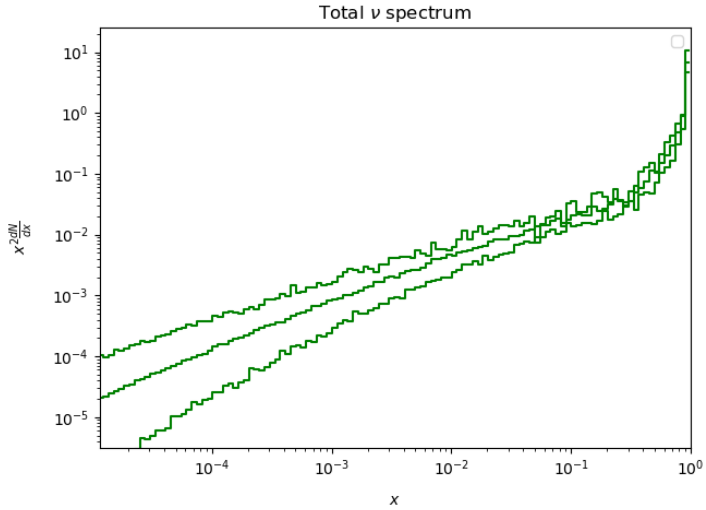

Figure 6.6: Neutrino spectra produced by our simulations. From top to bottom they correspond to dark matter masses of 10^{16} GeV, 10^{11} GeV and 10^{6} GeV respectively.

narrow, or abrupt feature (peak or knee) in the cosmic neutrino spectrum. Currently, IceCube data is not resolved enough to confirm or refute such features. The flux measured by IceCube can nevertheless be used to place limits on dark matter paramters, based on simulations such as ours. See for example reference [4].

Another thing to pay attention to is the seeming relative insignificance of the Z boson compared to the W boson in the cascading process. This is indicated by the compartively low proportions of energy that are carried away by the former compared to the latter (see table 6.1. To emphasize this point, we compare the preference of splitting channels of the right-handed electron to those of the left-handed electron in figure 6.7. It is clear that a significant proportion of left-handed electron's splittings produce weak bosons. However, the right-handed electron has a much higher probability of radiating away its energy in the form of photons, rather than the Z boson. This suggests that chiral physics may be important to the outcome of particle cascades. As an illustrative example, the direct coupling of a

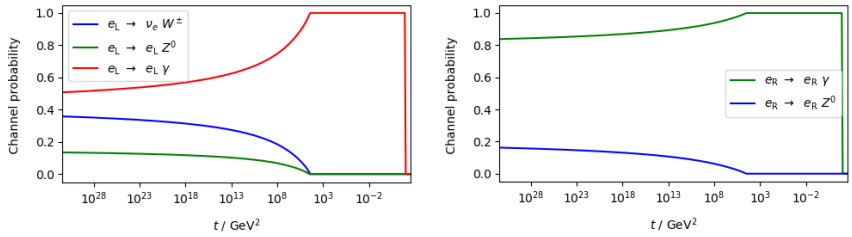

(a) (b)

Figure 6.7: Comparison between the splitting channels of a left-handed and right-handed electron. The right handed electron emits weak radiation in much lower proportions than the left-handed electron, due to not coupling to the W boson. The channel probabilities are proportional to $f(t)$ from equation (4.58).

dark matter to right handed electrons may not produce the abundance of cascading weak bosons that we predicted earlier. This may be an interesting concept to analyse further, in particular because earlier cascading models have ignored the particle chiralities [4, 8].

Lastly, we note that the spectra that our simulations predict for weak bosons and neutrinos are at odds with earlier results in ref.[8], see figure 6.8. We do not go into a discussion on this, as it would require more detailed insight into the models that have been used in those studies. However, we also note that our neutrino spectra correspond satisfactorally to the ones found by the authors of [4].

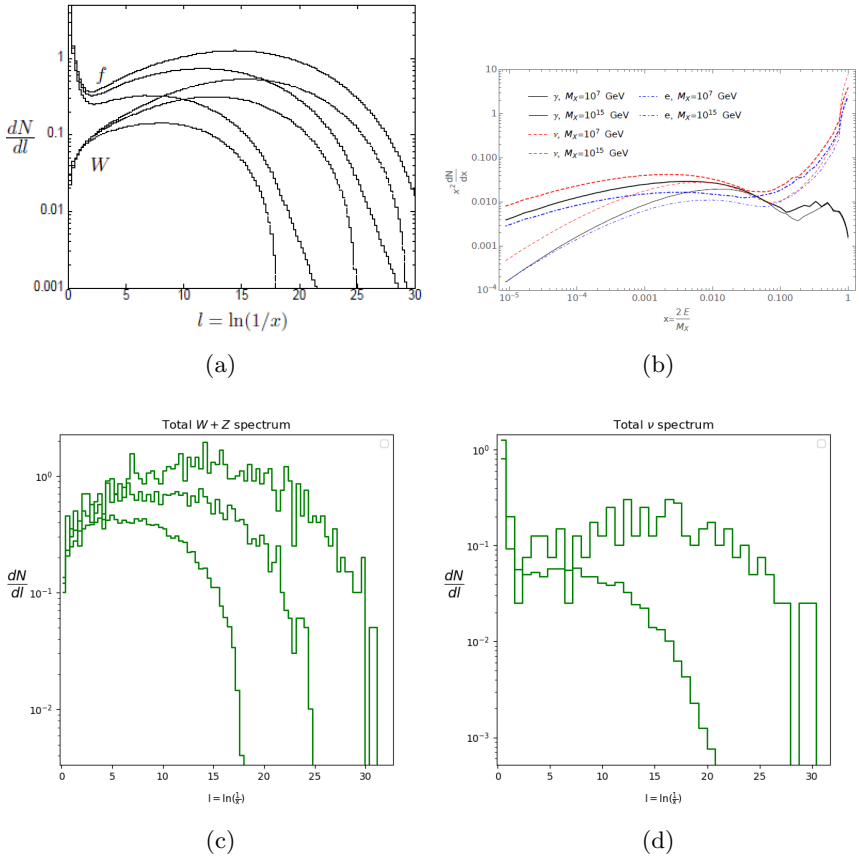

Figure 6.8: Neutrino and weak boson spectra found by other authors compared to our simulations. a illustrates the weak boson spectra found by the authors of ref. [8] for dark matter masses of 10^{16} GeV, 10^{13} GeV and 10^{10} GeV from top to bottom. We try to reproduce this in c, but get normalizations that are significantly larger. Similarly, we get much smaller normalizations for the neutrino spectra in d. The neutrino spectra in b [4] correspond well to our spectra form figure 6.6 on the high-energy end. For lower energies, the spectra differ due to our neglect of hadronization.

Chapter 7

Summary and Outlook

In this thesis, we have devised a scheme to simulate particle cascades with energies in the range between $10^6\,\mathrm{GeV}$ to $10^{16}\,\mathrm{GeV}$. We have taken into account both strong and electroweak interactions, and included every particle of the standard model (except the Higgs particle), distinguishing between left-chiral and right-chiral fermions. Given the generality of the cascading process, our simulation is applicable to predicting particle spectra from SHDM decay, and assumes about dark matter only that it decays into a pair of standard model particles, which is a non-restrictive assumption.

The case for this investigation was made, based on the status of neutrino astronomy and current understanding of dark matter. We reviewed a formalism of particle cascades, that is well known from QCD, and showed that the formalism can be defined in terms of splitting functions, which we derived in detail. These derivations formed the basis from which we determined the splitting functions for electroweak splittings. We found that all of the splitting functions (including those for strong interactions) have one of three forms, corresponding to triple boson splits, pair production or boson emission, because the Feynman rules for these types of splittings have the same forms, up to some scalar factors. Hence, the functions corresponding to the same categories of splittings only differed by scalar coefficients, which we determined. We also identified three random variables that define each splitting: the virtuality of the parent particle, the splitting channel, and the share of energy received by each produced particle. We determined the expressions for the probability distributions of these random variables. We also described how the decay of on-shell particles, hadronization and subsequent decay of partons could be included in our model, but were not able to account for tau decays. We argued that these were not expected to add discernible features to the final neutrino spectrum.

We continued by introducing the mathematics behind Monte Carlo algorithms that were appropriate for our task. A concrete account was given of the way in which these algorithms were applied to the background theory, so that our simulations would be a sound reflection of the physical processes.

The simulation was applied to pure gluon and parton cascades, the results compared to earlier work on similar simulations of parton jets. We found that

our results for pure gluon cascades were very similar to those of the earlier work, indicating the validity of our computer program. Gluon multiplicities and ratios between multiplicities from quark- and gluon-induced cascades also corresponded well to expectations. We demonstrated that the dominance of the strong coupling over the electroweak coupling implies that in any cascade, the appearance of partons starts purely partonic sub-cascades, thus effectively dividing the cascade into an electroweak part and separate QCD parts.

Our simulation of hadronizing parton cascades did not correspond well to the empirical pion spectrum. This is probably because the phenomenological hadronization functions that the model depends on assume different quark spectra than what our simulation predicts. As the determination of hadronization functions is beyond the scope of our own work, this effectively prevented us from taking hadronization into account in our simulations. We therefore didn't investigate the dark matter-to-partons decay channel, seeing as practically all of its products were expected to hadronize. This problem may be worth looking at more closely, seeing as hadronic decay channels may produce neutrino spectra that are qualitatively very different to those of the leptonic decay channels.

The leptonic decay channels of dark matter were studied in some more detail. We argued that the resulting cascades are dominated by W and Z boson production, and that the final spectra are hence produced in large parts by the decays of these. This should in principle make the cascade results relatively independent of the starting particle. We found however, that a starting neutrino causes a sharp peak at the high-end of its own energy spectrum, corresponding to the dark matter decays for which a primary neutrino does not split (or emits too few bosons to lose significant amounts of its own energy). This dominance of primary, highly-energetic neutrinos is still prevalent for decays of the most massive dark matter particles considered. Hence, the dark matter-to-neutrinos decay channel would be likely to produce visible signals in neutrino data, corresponding to sharp features such as narrow peaks. The identification of such features seems however unlikely, given the low resolution in IceCube data so far. Simulations such as ours can nevertheless be used to place limits on dark matter parameters.

We found that our simulated spectra of neutrinos and weak bosons correspond well to the simulations of some authors, but are at odds with others.

We have focused mostly on the spectrum of neutrinos that our simulations predict for dark matter decay. The reason for this is partly because neutrino spectra are most easily compared with observations, seeing as photon spectra would need to take into account attenuation effects due to background media. In addition, photon spectra are expected to be dominated by pion decay, which we haven't been able to take into account in this work. However, in principle, our model makes predictions for gamma ray spectra as well. In the near future, a larger wealth of IceCube data will reveal more accurate spectra and distributions of cosmic neutrinos, and hopefully allow for a determination of the extent to which the neutrino flux is galactic in origin. A galactic flux would have direct implications for the gamma ray flux' relationship to the neutrino flux, and the two can be compared in both observations and simulations. This could truly unlock the potential of multi

messenger astronomy.

Bibliography

[1] M. Ahlers and F. Halzen, "IceCube: Neutrinos and multimessenger astronomy," *Progress of Theoretical and Experimental Physics*, vol. 2017, 11 2017. 1, 2.1, 2.1, 2.1, 2.2.1, 2.2.1, 2.1, 4, 2.2.1, 2.3, 2.2.2, 2.2.2

[2] V. A. Kuzmin and V. A. Rubakov, "Ultrahigh-energy cosmic rays: A Window to postinflationary reheating epoch of the universe?," *Phys. Atom. Nucl.*, vol. 61, p. 1028, 1998. 1, 2.1

[3] V. A. Kuzmin and I. I. Tkachev, "Ultra-high-energy cosmic rays and inflation relics," *Physics Reports*, vol. 320, no. 1, pp. 199 – 221, 1999. 2.1

[4] M. Kachelrieß, O. E. Kalashev, and M. Y. Kuznetsov, "Heavy decaying dark matter and IceCube high energy neutrinos," *Phys. Rev. D*, vol. 98, p. 083016, Oct 2018. 1, 2.1, 6.2, 6.2, 6.2, 6.8

[5] R. Aloisio, V. Berezinsky, and M. Kachelriess, "On the status of superheavy dark matter," *Phys. Rev.*, vol. D74, p. 023516, 2006. 1, 2.1, 3.2

[6] W. H. Kinney, "TASI Lectures on Inflation," 2009. 1, 3.2

[7] E. W. Kolb, D. J. H. Chung, and A. Riotto, "WIMPzillas!," *AIP Conf. Proc.*, vol. 484, no. 1, pp. 91–105, 1999. [,592(1999)]. 1, 3.2

[8] V. Berezinsky, M. Kachelriess, and S. Ostapchenko, "Electroweak Jet Cascading in the Decay of Superheavy Particles," *Physical review letters*, vol. 89, p. 171802, 11 2002. 1, 2.1, 4.3, 4.3.1, 4.3.1, 6.2, 6.2, 6.8

[9] O. Pisanti, "Cosmic Neutrinos," *PoS*, vol. NuFact2017, p. 024, 2017. 2.1, 2.1

[10] F. Halzen and U. Katz, "The era of kilometer-scale neutrino detectors," *Adv. High Energy Phys.*, vol. 2013, p. 680584, 2013. 2.1, 2.1, 2.1, 2.2, 2.2.1, 2.2.1, 2.2.1

[11] A. De Angelis and M. Mallamaci, "Gamma-Ray Astrophysics," *Eur. Phys. J. Plus*, vol. 133, p. 324, 2018. 2.1

[12] F. Aharonian, A. Bykov, E. Parizot, V. Ptuskin, and A. Watson, "Cosmic Rays in Galactic and Extragalactic Magnetic Fields," *Space Science Reviews*, vol. 166, pp. 97–132, May 2012. 2.1

[13] E. G. Zweibel, "The microphysics and macrophysics of cosmic rays," *Physics of Plasmas*, vol. 20, 05 2013.

[14] P. Desiati and E. G. Zweibel, "," *The Astrophysical Journal*, vol. 791, p. 51, jul 2014. 2.1

[15] G. T. Zatsepin and V. A. Kuzmin, "Upper limit of the spectrum of cosmic rays," *JETP Lett.*, vol. 4, pp. 78–80, 1966. [Pisma Zh. Eksp. Teor. Fiz.4,114(1966)]. 2.1

[16] "Neutrino emission from the direction of the blazar TXS 0506+056 prior to the IceCube-170922A alert," *Science*, vol. 361, no. 6398, pp. 147–151, 2018. 2.1

[17] A. Keivani *et al.*, "A Multimessenger Picture of the Flaring Blazar TXS 0506+056: implications for High-Energy Neutrino Emission and Cosmic Ray Acceleration," *Astrophys. J.*, vol. 864, no. 1, p. 84, 2018. 2.1

[18] M. Cerruti, A. Zech, C. Boisson, G. Emery, S. Inoue, and J.-P. Lenain, "Gammas and neutrinos from TXS 0506+056," 10 2018. 2.1

[19] S. Ansoldi *et al.*, "The blazar TXS 0506+056 associated with a high-energy neutrino: insights into extragalactic jets and cosmic ray acceleration," *Astrophys. J. Lett.*, 2018. [Astrophys. J.863,L10(2018)]. 2.1

[20] M. Agostini, K. Altenmüller, S. Appel, V. Atroshchenko, Z. Bagdasarian, D. Basilico, G. Bellini, J. Benziger, D. Bick, G. Bonfini, D. Bravo, B. Caccianiga, F. Calaprice, A. Caminata, S. Caprioli, M. Carlini, P. Cavalcante, A. Chepurnov, and K. Choi, "Comprehensive measurement of pp-chain solar neutrinos," *Nature*, vol. 562, pp. 505–510, 10 2018. 1

[21] Ken'ichiro Nakazato and Kohsuke Sumiyoshi and Hideyuki Suzuki and Tomonori Totani and Hideyuki Umeda and Shoichi Yamada, "SUPERNOVA NEUTRINO LIGHT CURVES AND SPECTRA FOR VARIOUS PROGENITOR STARS: FROM CORE COLLAPSE TO PROTO-NEUTRON STAR COOLING," *The Astrophysical Journal Supplement Series*, vol. 205, p. 2, feb 2013.

[22] I. Tamborra, B. Mueller, L. Huedepohl, H.-T. Janka, and G. Raffelt, "High-resolution supernova neutrino spectra represented by a simple fit," *Physical Review D*, vol. 86, 11 2012. 1

[23] P. Meszaros, "Astrophysical Sources of High Energy Neutrinos in the IceCube Era," *Ann. Rev. Nucl. Part. Sci.*, vol. 67, pp. 45–67, 2017. 2.1, 2.1

[24] P. Blasi, "The Origin of Galactic Cosmic Rays," *Nuclear Physics B - Proceedings Supplements*, vol. s 239–240, 11 2012. 2.1

[25] V. Berezinsky, M. Kachelriess, and A. Vilenkin, "Ultrahigh-energy cosmic rays without GZK cutoff," *Phys. Rev. Lett.*, vol. 79, pp. 4302–4305, 1997. 2.1

[26] V. G. Macías, J. Illana, and J. Wudka, "," *Journal of Physics: Conference Series*, vol. 761, p. 012082, oct 2016. 2.1

[27] V. Gonzalez Macias and J. Wudka, "Effective theories for Dark Matter interactions and the neutrino portal paradigm," *JHEP*, vol. 07, p. 161, 2015.

[28] M. Blennow, E. Fernandez-Martinez, A. O.-D. Campo, S. Pascoli, S. Rosauro-Alcaraz, and A. V. Titov, "Neutrino Portals to Dark Matter," 2019. 2.1

[29] S. Bilenky, "Neutrino oscillations: From a historical perspective to the present status," *Nuclear Physics B*, vol. 908, pp. 2 – 13, 2016. Neutrino Oscillations: Celebrating the Nobel Prize in Physics 2015. 2.1, 3.2

[30] A. Falkowski, J. Juknevich, and J. Shelton, "Dark Matter Through the Neutrino Portal," 2009. 2.1, 3.2

[31] M. G. e. a. Aartsen, "First Observation of PeV-Energy Neutrinos with IceCube," *Phys. Rev. Lett.*, vol. 111, p. 021103, Jul 2013. 2.2

[32] M. G. e. a. Aartsen, "Observation of High-Energy Astrophysical Neutrinos in Three Years of IceCube Data," *Phys. Rev. Lett.*, vol. 113, p. 101101, Sep 2014. 2.2

[33] A. Karle, "IceCube," 2010. 2.2, 2.2.1, 2.2.1

[34] M. G. Aartsen *et al.*, "Energy Reconstruction Methods in the IceCube Neutrino Telescope," *JINST*, vol. 9, p. P03009, 2014. 2.2.1

[35] M. G. Aartsen *et al.*, "The IceCube Neutrino Observatory - Contributions to ICRC 2017 Part II: Properties of the Atmospheric and Astrophysical Neutrino Flux," 2017. 2.2

[36] J. Auffenberg, "IceTop as a veto in astrophysical neutrino searches for IceCube," in *Proceedings, 33rd International Cosmic Ray Conference (ICRC2013): Rio de Janeiro, Brazil, July 2-9, 2013*, p. 0373. 2.2.1

[37] K. Murase, M. Ahlers, and B. C. Lacki, "Testing the Hadronuclear Origin of PeV Neutrinos Observed with IceCube," *Phys. Rev.*, vol. D88, no. 12, p. 121301, 2013. 2.2.2

[38] A. Neronov and D. Semikoz, "Neutrinos from Extra-Large Hadron Collider in the Milky Way," *Astropart. Phys.*, vol. 72, pp. 32–37, 2016. 2.2.2

[39] A. Neronov, M. Kachelrieß, and D. V. Semikoz, "Multimessenger gamma-ray counterpart of the IceCube neutrino signal," *Phys. Rev.*, vol. D98, no. 2, p. 023004, 2018. 2.2.2

[40] A. Neronov and D. V. Semikoz, "Evidence the Galactic contribution to the IceCube astrophysical neutrino flux," *Astropart. Phys.*, vol. 75, pp. 60–63, 2016. 2.2.2

[41] G. Bertone and D. Hooper, "History of dark matter," *Rev. Mod. Phys.*, vol. 90, no. 4, p. 045002, 2018. 3.1

[42] Y. Sofue and V. Rubin, "Rotation Curves of Spiral Galaxies," *Annual Review of Astronomy and Astrophysics*, vol. 39, no. 1, pp. 137–174, 2001. 3.1

[43] D. Clowe, M. Bradac, A. H. Gonzalez, M. Markevitch, S. W. Randall, C. Jones, and D. Zaritsky, "A direct empirical proof of the existence of dark matter," *Astrophys. J.*, vol. 648, pp. L109–L113, 2006. 3.1

[44] J. F. Navarro, C. S. Frenk, and S. D. M. White, "A Universal density profile from hierarchical clustering," *Astrophys. J.*, vol. 490, pp. 493–508, 1997. 3.1

[45] F. Iocco, M. Pato, G. Bertone, and P. Jetzer, "Dark Matter distribution in the Milky Way: microlensing and dynamical constraints," *JCAP*, vol. 1111, p. 029, 2011. 3.1

[46] D. Hooper, "The Density of Dark Matter in the Galactic Bulge and Implications for Indirect Detection," *Physics of the Dark Universe*, vol. 15, 07 2016. 3.1

[47] D. J. H. Chung, P. Crotty, E. Kolb, and A. Riotto, "Gravitational production of superheavy dark matter," *Physical Review D*, vol. 64, 05 2001. 3.2

[48] F. S. Queiroz, "WIMP Theory Review," *PoS*, vol. EPS-HEP2017, p. 080, 2017. 3.2

[49] J. L. Feng, "Naturalness and the Status of Supersymmetry," *Ann. Rev. Nucl. Part. Sci.*, vol. 63, pp. 351–382, 2013. 3.2

[50] R. D. Peccei, "The Strong CP problem and axions," *Lect. Notes Phys.*, vol. 741, pp. 3–17, 2008. [,3(2006)]. 3.2

[51] A. Boyarsky, M. Drewes, T. Lasserre, S. Mertens, and O. Ruchayskiy, "Sterile Neutrino Dark Matter," *Prog. Part. Nucl. Phys.*, vol. 104, pp. 1–45, 2019. 3.2

[52] L. Kofman, A. D. Linde, and A. A. Starobinsky, "Reheating after inflation," *Phys. Rev. Lett.*, vol. 73, pp. 3195–3198, 1994. 3.2

[53] R. Allahverdi, R. Brandenberger, F.-Y. Cyr-Racine, and A. Mazumdar, "Reheating in Inflationary Cosmology: Theory and Applications," *Ann. Rev. Nucl. Part. Sci.*, vol. 60, pp. 27–51, 2010. 3.2

[54] S. Hashiba and J. Yokoyama, "Gravitational particle creation for dark matter and reheating," *Phys. Rev.*, vol. D99, no. 4, p. 043008, 2019. 3.2

[55] Y. Ema, R. Jinno, K. Mukaida, and K. Nakayama, "Gravitational particle production in oscillating backgrounds and its cosmological implications," *Phys. Rev. D*, vol. 94, p. 063517, Sep 2016. 3.2

[56] Y. Tang and Y.-L. Wu, "On thermal gravitational contribution to particle production and dark matter," *Physics Letters B*, vol. 774, pp. 676 – 681, 2017.

[57] Y. Ema, K. Nakayama, and Y. Tang, "Production of Purely Gravitational Dark Matter," *JHEP*, vol. 09, p. 135, 2018. 3.2

[58] A. Gangui, "Topological defects in cosmology," 2001. 2

[59] A. Deur, S. J. Brodsky, and G. F. de Teramond, "The QCD Running Coupling," *Prog. Part. Nucl. Phys.*, vol. 90, pp. 1–74, 2016. 4.1.1

[60] M. Kachelriess, *Quantum Fields*. Oxford Graduate Texts, Oxford University Press, 2017. 4.1.1, 4.1.3

[61] J. C. Romao and J. P. Silva, "A resource for signs and Feynman diagrams of the Standard Model," *Int. J. Mod. Phys.*, vol. A27, p. 1230025, 2012. 4.1.3, 4.1.3, 4.1.3, 4.3.2

[62] G. Marchesini and B. Webber, "," *Nuclear Physics B*, vol. 238, no. 1, pp. 1 – 29, 1984. 4.2, 4.2, 4.2, 6.1, 6.2, 6.1, 6.1

[63] M. Tanabashi *et al.*, "Review of Particle Physics," *Phys. Rev.*, vol. D98, no. 3, p. 030001, 2018. 4.3, 4.4.1

[64] V. Berezinsky and M. Kachelriess, "Monte Carlo simulation for jet fragmentation in SUSY QCD," *Phys. Rev.*, vol. D63, p. 034007, 2001. 4.4.2, 4.4.3, 4.4.3, 4.4.3

[65] R. Aloisio, V. Berezinsky, and M. Kachelriess, "Fragmentation functions in SUSY QCD and UHECR spectra produced in top - down models," *Phys. Rev.*, vol. D69, p. 094023, 2004. 4.4.3

[66] T. Sjostrand, "PYTHIA 5.7 and JETSET 7.4: Physics and manual," 1994. 5.1, 5.1

[67] B. Webber, "A QCD model for jet fragmentation including soft gluon interference," *Nuclear Physics B*, vol. 238, no. 3, pp. 492 – 528, 1984. 6.1

NTNU
Norwegian University of
Science and Technology